# $Mn^{I}$ Complex Redox Potential Tunability by Remote Lewis Acid Interaction.

Anandi Srinivasan,[a] Jesús Campos,[b] Nicolas Giraud,[c] Marc Robert,[a,d] Orestes Rivada–Wheelaghan[a]*

[a] Université de Paris, Laboratoire d'Electrochimie Moléculaire, CNRS, F-75013 Paris, France.

[b] Instituto de Investigaciones Químicas (IIQ), Consejo Superior de Investigaciones Científicas (CSIC) and University of Sevilla. Avenida Américo Vespucio 49, 41092 Sevilla (Spain).

[c] Université de Paris, Laboratoire de Chimie et Biochimie Pharmacologiques et Toxicologiques, UMR CNRS 8601, Paris, France.

[d] Institut Universitaire de France (IUF), F-75005 Paris, France.

**Table of Contents**

## I. General specifications

All manipulations unless stated otherwise were performed using Schlenk or glovebox techniques under dry argon or nitrogen atmosphere, respectively. THF and diethyl ether were dried over Na/benzophenone, freshly distilled prior to use and stored under nitrogen atmosphere over molecular sieves (4Å). Anhydrous deuterated solvents were purchased from Eurisotop and stored over 4Å molecular sieves. All chemicals unless noted otherwise were purchased from major commercial suppliers (TCI, Sigma-Aldrich) and used as received.

**NMR spectra** were measured on a Bruker Avance II 400 MHz spectrometer. The following abbreviations are used for describing NMR spectra: s (singlet), d (doublet), t (triplet), td (triplet of doublets), ddd (doublet of doublets of doublets), vd (virtual doublet), vt (virual triplet), br (broad). Electrospray Ionization Mass Spectrometry (ESI-MS) measurements were performed on a Bruker apparatus. FT-IR spectra were measured using Perkin-Elmer FT-IR spectrometer. The following abbreviations are used for describing FT-IR spectra: s (strong), m (medium), w (weak), br (broad). Absorbance spectra were collected using an Agilent cary 60 UV-vis instrument.

**CV experiments** were carried out using an AUTOLAB potentiostat (Meterohm) with three electrode system, containing 0.1 M TBAH electrolyte solution in anhydrous DMF. A glassy carbon disk (3 mm diameter) was employed as a working electrode with a platinum (Pt) wire as a counter electrode and a SCE as a reference electrode, separated from the solution by a porous frit. Prior to each measurement, the working electrode was polished with diamond paste (0.25 µm particle size) and rinsed with acetone and ultrapure water (>18.2 MΩ $cm^{-1}$, Millipore Milli-Q) and, after which it was sonicated for 2 mins in ultrapure water and dried before use.

## II. Experimental Procedures

### a. Ligand Synthesis and Characterization (L1-HBr)

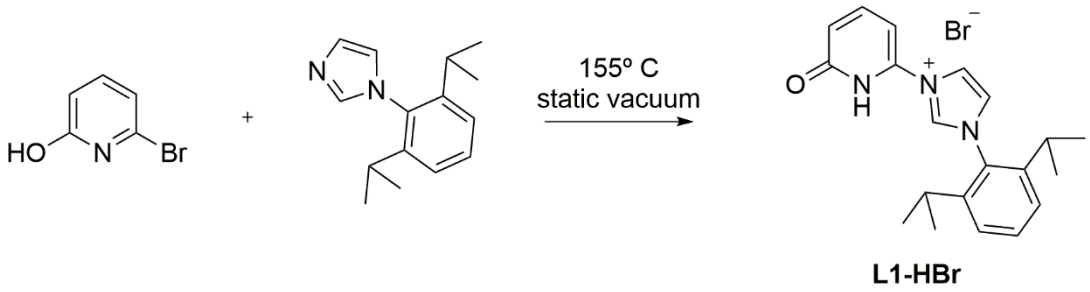


**L1-HBr**

**Scheme S1**. Formation of ligand **L1-HBr**.

*Synthesis:*

Inside the glovebox, 2-bromo-6-hydroxypyridine (500 mg, 2.87 mmol) and 1-(2,6-diisopropylphenyl) imidazole (655 mg, 2.87 mmol) where placed in a Teflon capped ampule together with a stirring bar. The ampule was sealed under vacuum, removed from the glovebox and stirred at 155 ºC for 5 days. After the 5 days, the ampule was left to cool to RT and the solid was washed with diethyl ether and ethyl acetate, yielding 690 mg (60 % yield) of pure **L1-HBr**.

*Characterization:*

$^{1}$H NMR (400 MHz, 20 ºC, $CDCl_3$) δ: 10.33 (br s, 2H, N-H and $CH_{NHC}$), 9.12 (br s, 1H, *backbone*-$CH_{NHC}$), 7.97 (br s, 1H, *4*-$CH_{Py}$), 7.72 (br s, *3*-$CH_{Py}$), 7.57 (br s, *para*-$CH_{diip}$) 7.40 (br s, *backbone*-$CH_{NHC}$), 7.34 (d, $^{3}J_{H,H}$ = 7.9 Hz, 2H, *meta*-$CH_{diip}$), 6.95 (d, $^{3}J_{H,H}$ = 8.2 Hz, 1H, *2*-$CH_{Py}$), 2.40 (quint, $^{3}J_{H,H}$ = 6.8 Hz, 2H, C<u>*H*</u>$(CH_3)_2$), 1.25 (d, $^{3}J_{H,H}$ = 6.8 Hz, 6H, CH(C<u>*H*</u>$_3)_2$), 1.17 (d, $^{3}J_{H,H}$ = 6.8 Hz, 6H, CH(C<u>*H*</u>$_3)_2$).

$^{13}$C{$^{1}$H} NMR (101 MHz, 20 ºC, $CDCl_3$) δ: 163.8 (Cq, *1*-$C_{Py}$), 145.6 (Cq, *orto*-$C_{diip}$), 143.7 (Cq, *5*-$C_{Py}$), 142.5 (CH, *3*-$CH_{Py}$), 135.6 (CH, $CH_{NHC}$), 132.4 (CH, *para*-$CH_{diip}$), 130.5 (Cq, *ipso*-$CH_{diip}$), 125.7 (CH, *backbone*-$CH_{NHC}$), 125.1 (CH, *meta*-$CH_{diip}$), 121.3 (CH, *backbone*-$CH_{NHC}$), 112.5 (CH, *2*-$CH_{Py}$), 106.1 (CH, *4*-$CH_{Py}$), 29.1 (CH, <u>*C*</u>H$(CH_3)_2$), 24.5 and 24.4 ($CH_3$, CH(<u>*C*</u>$H_3)_2$), 10.44.

ESI-HRMS (m/z pos): Found (Calc): $C_{20}H_{24}N_3O^+$ 322.1906 (322.1914).

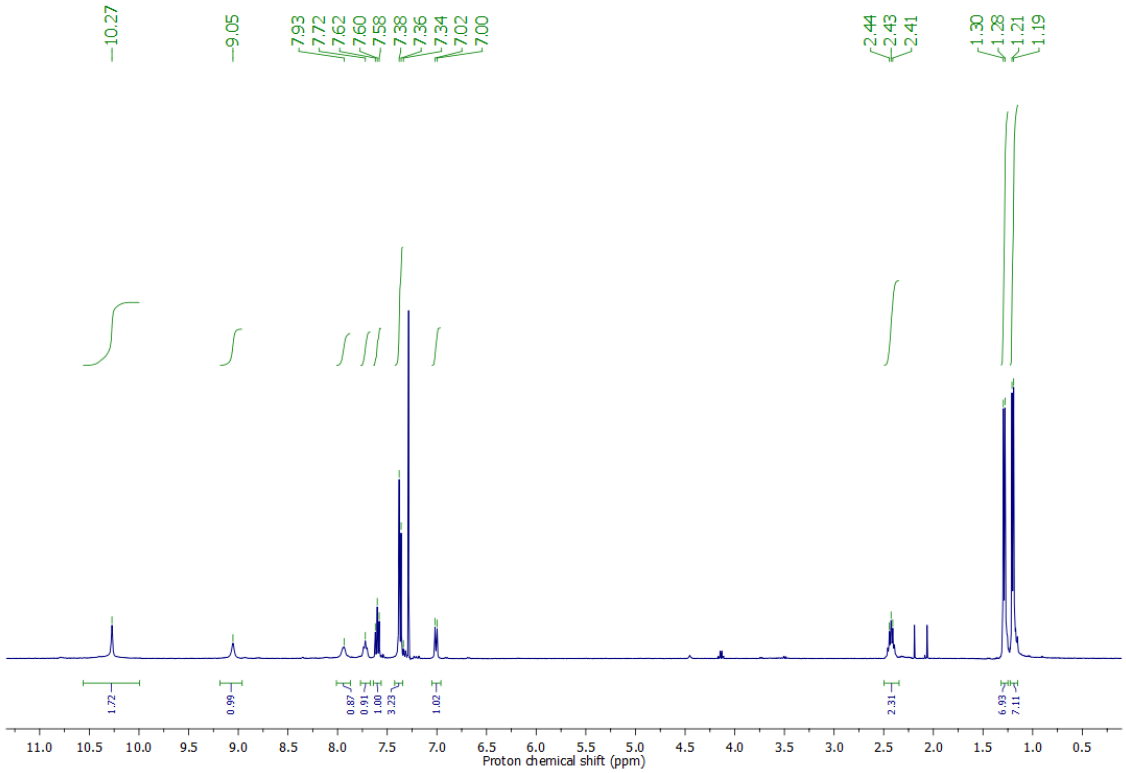


**Figure S1**. $^1$H NMR spectrum (400 MHz). $CDCl_3$ solution containing ligand **L1-HBr**.

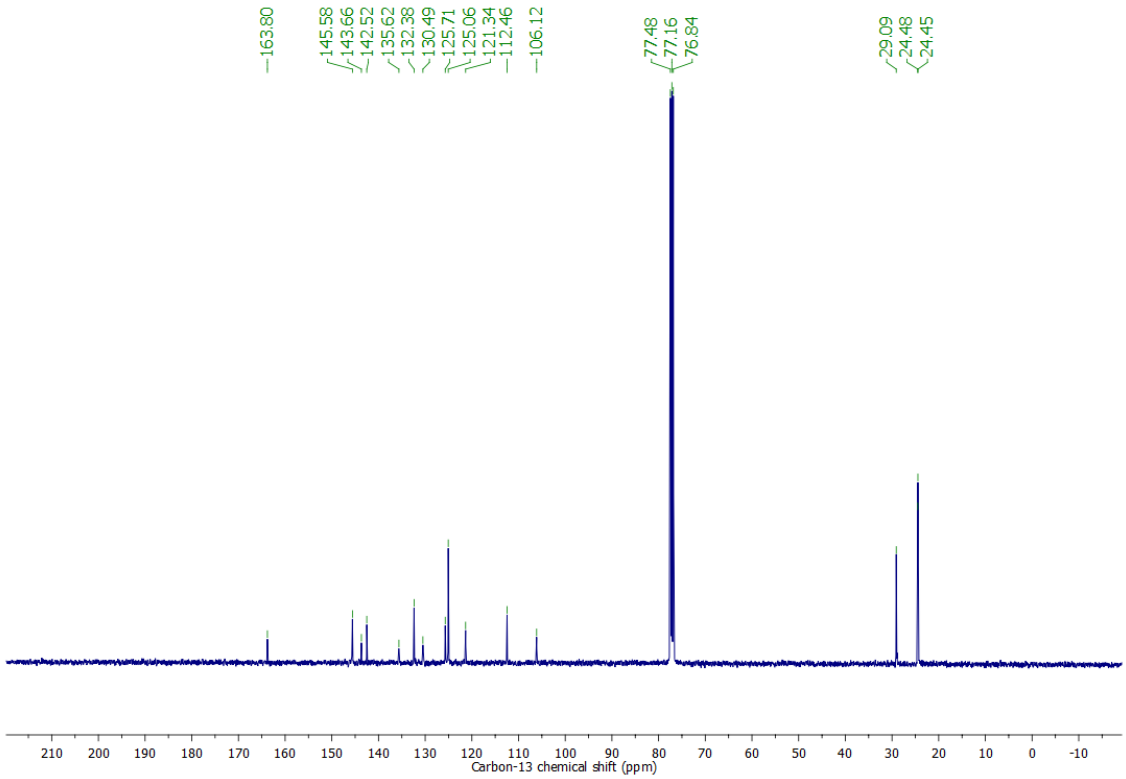


**Figure S2**. $^{13}$C-{$^1$H} spectrum (400 MHz). $CDCl_3$ solution containing **L1-HBr**.

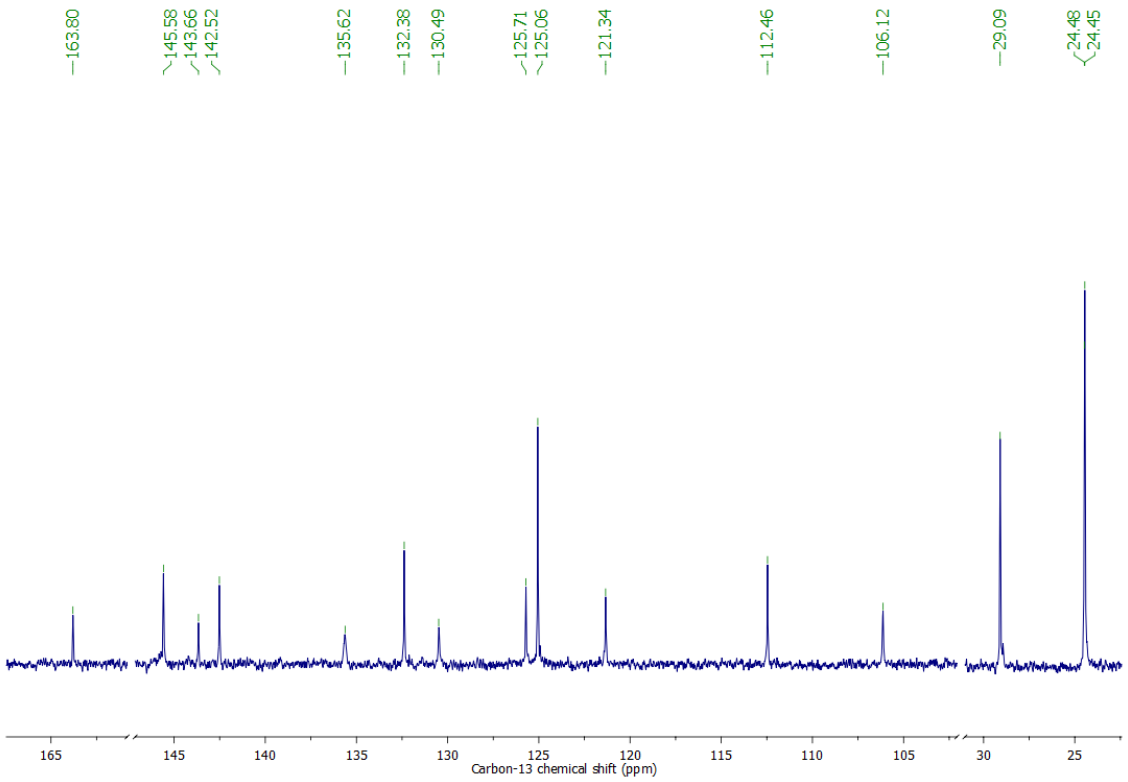


**Figure S3**. $^{13}C$-{$^{1}H$} spectrum (400 MHz - zoomed). $CDCl_3$ solution containing **L1-HBr**.

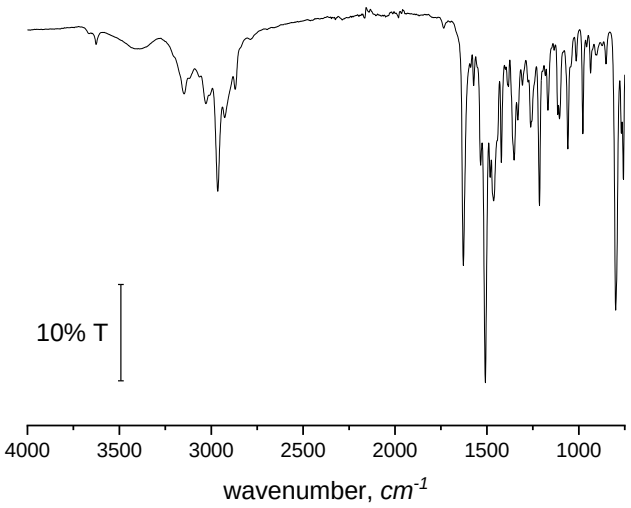


**Figure S4**. ATR FT-IR transmittance spectrum of **L1-HBr**.

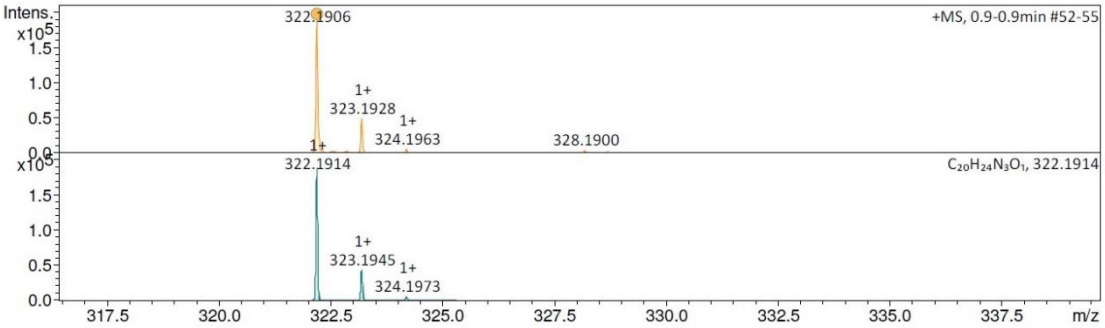


**Figure S5**. ESI-(HR)MS spectrum of MeOH solution of **L1-HBr** (top) and simulated spectrum for $C_{20}H_{24}N_3O^+$ and $C_{20}H_{23}N_3O^+$ (below).

### b. Complex Synthesis and characterization (1)

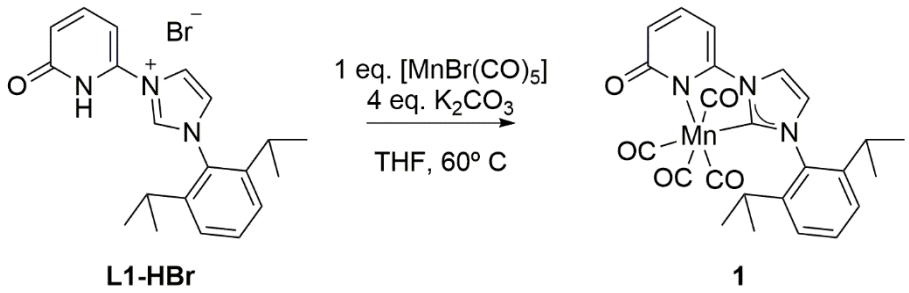


**Scheme S2**. Formation of complex **1**.

*Synthesis:*

Inside the glovebox, ligand **L1-HBr** (114 mg, 0.28 mmol), metal precursor $[MnBr(CO)_5]$ (78 mg, 0.28 mmol), and $K_2CO_3$ (200 mg, 1.45 mmol), were placed in a Teflon capped ampule and the solid were dissolved in dry THF (10 mL). Once out the glovebox, the solution was put to stir at 60 ºC for 18h. Later, the solution was filtered, and the solvent was removed under vacuum. The product was washed with cold diethyl ether (–40 °C) using Schlenk-technique canula filtration (92 mg, 76 % yield).

When unreactive imidazolium salt is present, warm extraction with toluene (60 ºC) can be used to obtain pure complex **1**. The complex can be crystallized by placing concentrated diethyl ether solutions of complex **1** in the freezer (–33 °C).

*Characterization:*

$^1$H NMR (400 MHz, 20 ºC, THF-$d_8$) δ: 8.31 (s, 1H, *backbone*-$CH_{NHC}$), 7.67 (d, $^3J_{H,H}$ = 1.4 Hz, 1H, *backbone*-$CH_{NHC}$), 7.61 – 7.53 (m, 1H, *para*-$CH_{diip}$), 7.43 (d, J = 7.8 Hz, 2H, *meta*-$CH_{diip}$), 7.23 (m, 1H, *4*-$CH_{Pynone}$), 6.52 (d, $^3J_{H,H}$ = 6.8 Hz, 1H, $CH_{Pynone}$), 6.09 (d, $^3J_{H,H}$ = 8.3 Hz, 1H, $CH_{Pynone}$), 2.68 (sept, $^3J_{H,H}$ = 6.8 Hz, 2H, C<u>H</u>$(CH_3)_2$), 1.36 (d, $^3J_{H,H}$ = 6.8 Hz, 6H, CH(C<u>H</u>$_3)_2$), 1.20 (d, $^3J_{H,H}$ = 6.8 Hz, 6H, CH(C<u>H</u>$_3)_2$).

$^{13}$C{$^1$H} NMR (101 MHz, 20 ºC, THF-$d_8$) δ: 216.00 ($C_q$, CO), 211.96 ($C_q$, CO), 210.45 ($C_q$, 2 CO), 193.60 ($C_q$, Mn-$C_{NHC}$), 168.77 ($C_q$, $C_{Pynone}$), 150.14 ($C_q$, $C_{Pynone}$), 146.15 ($C_q$, *orto*-$C_{diip}$), 136.19 (CH, *4*-$CH_{Pynone}$), 134.85 ($C_q$, *ipso*-$C_{diip}$), 130.72 (CH, *para*-

$CH_{diip}$), 127.75 (CH, *backbone*-$CH_{NHC}$), 124.10 (CH, *meta*-$CH_{diip}$), 117.42 (CH, *backbone*-$CH_{NHC}$), 112.91 (CH, $CH_{Pynone}$), 90.38 (CH, $CH_{Pynone}$), 28.34 (CH, $C\underline{H}(CH_3)_2$), 24.97 ($CH_3$, $CH(C\underline{H}_3)_2$), 21.96 ($CH_3$, $CH(C\underline{H}_3)_2$).

FTIR ($cm^{-1}$): 2013(br, s), 1994(br, m), 1924(br, s), 1900(s).

ESI-HRMS (m/z pos): Found (Calc): $C_{24}H_{23}MnN_3O5^+$ 488.0993 (488.1013)

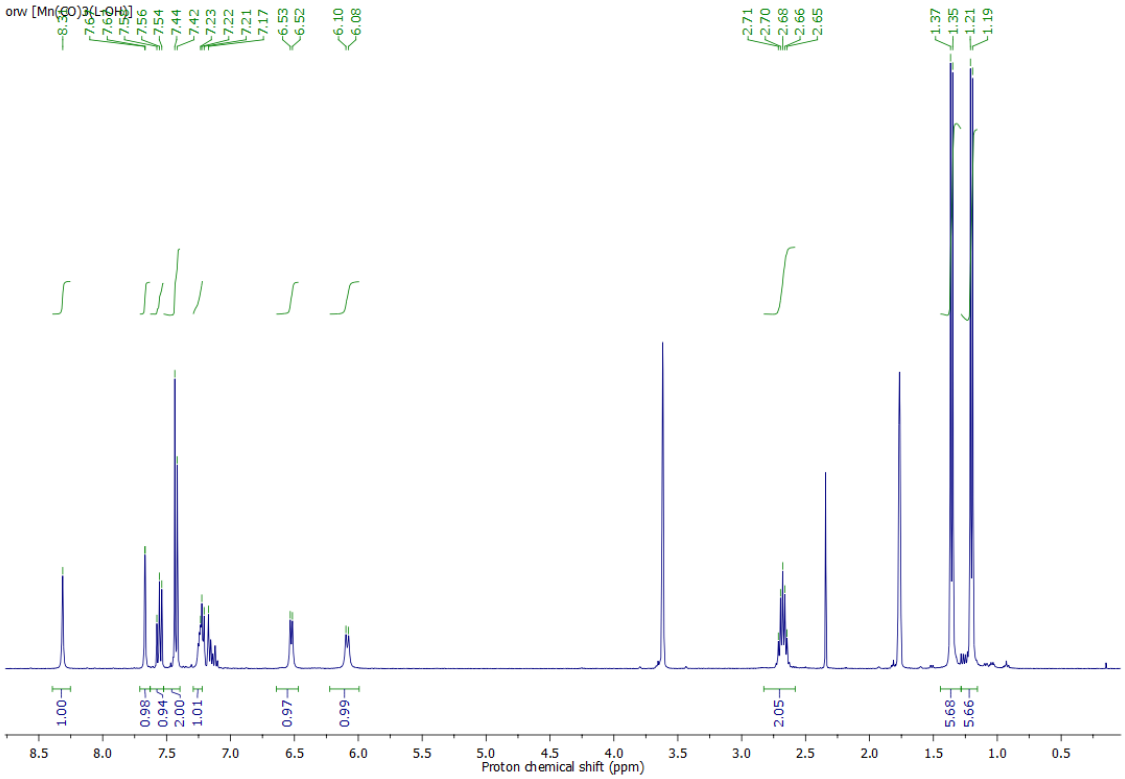


**Figure S6**. $^1$H NMR spectrum (400 MHz). THF-$d_8$ solution containing **1**.

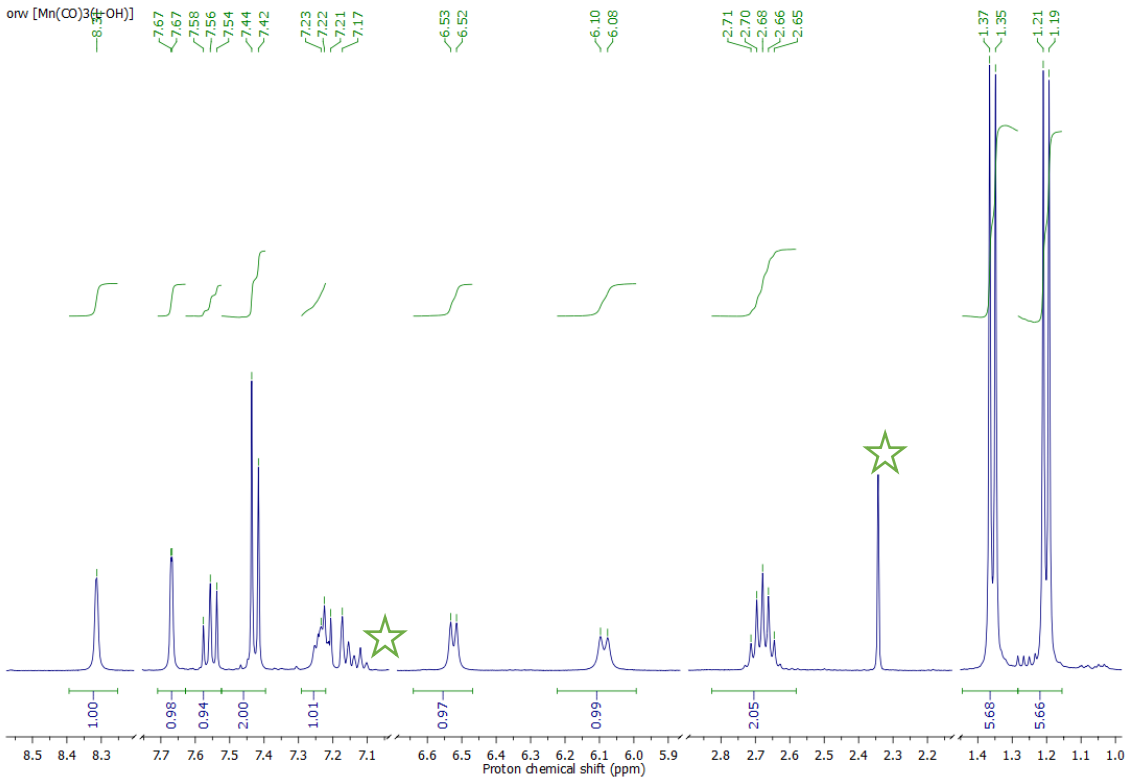


**Figure S7**. $^{1}$H NMR spectrum (400 MHz). (zoomed). THF-$d_8$ solution containing **1**. Green star highlight toluene-solvent peaks.

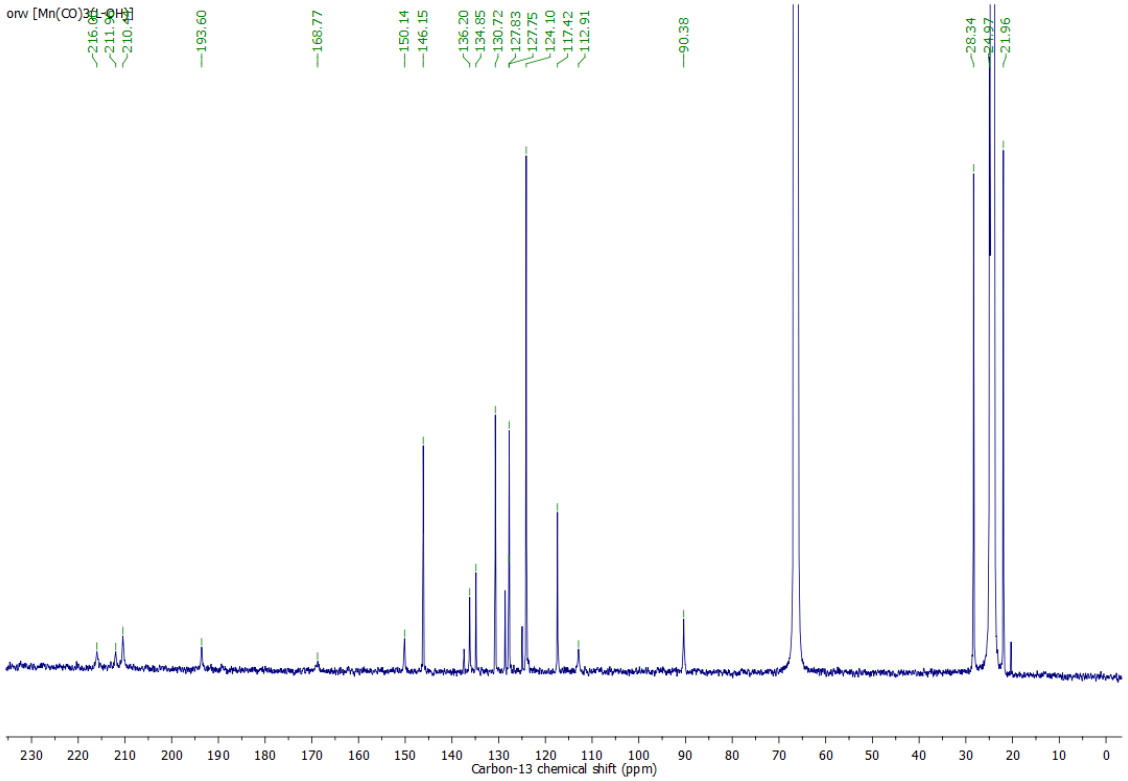


**Figure S8**. {$^{1}$H}$^{13}$C spectrum (400 MHz). THF-$d_8$ solution containing **1**.

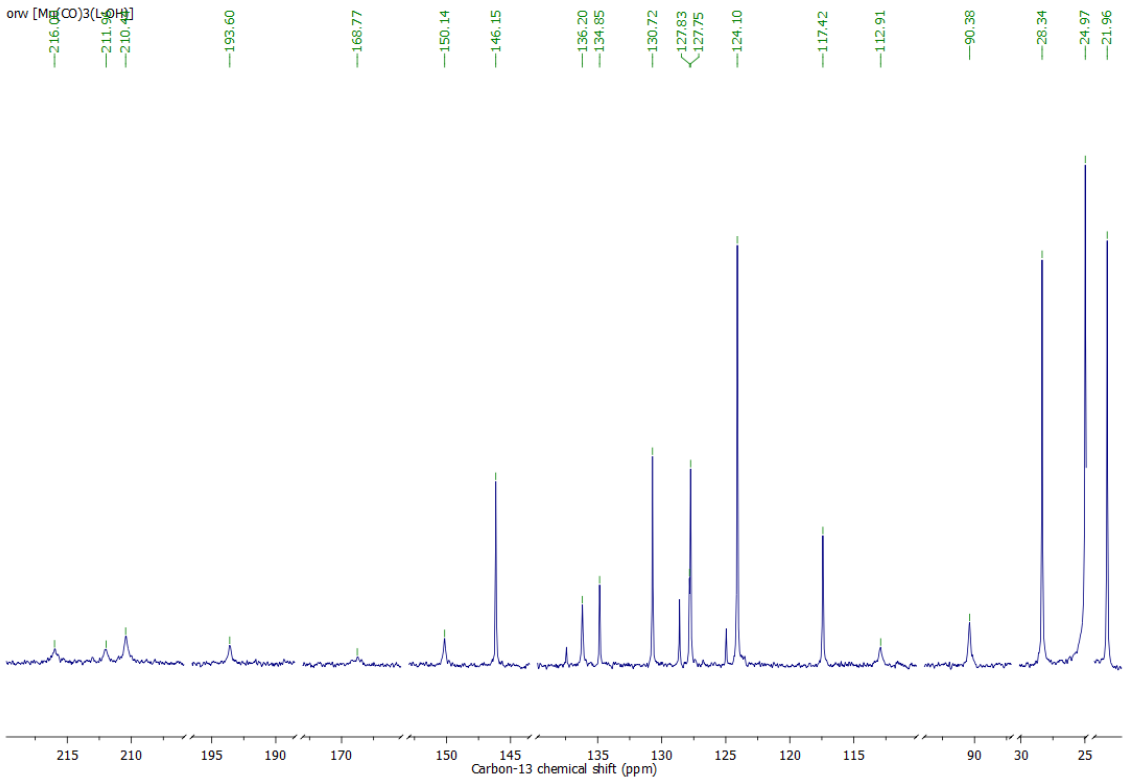


**Figure S9**. $^{13}C$-{$^{1}H$} spectrum (400 MHz - zoomed). THF-$d_8$ solution containing **1**.

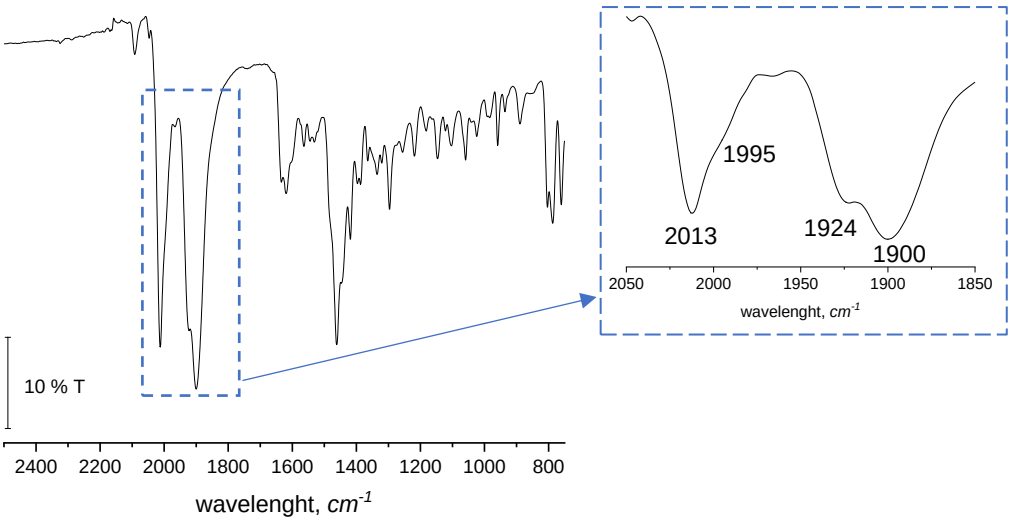


**Figure S10**. ATR FT-IR transmittance spectrum of **1**. CO bands highlighted in zoom.

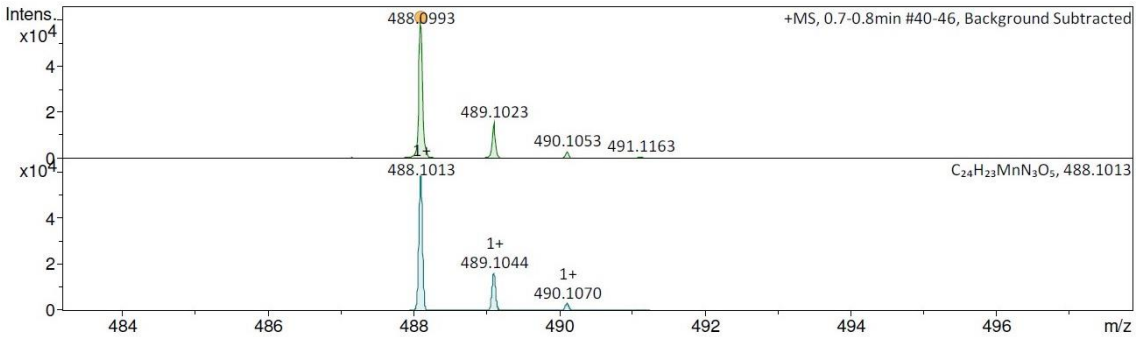


**Figure S11**. ESI-(HR)MS spectrum of $CH_2Cl_2$ solution of **1** (top) and simulated spectrum for $C_{24}H_{23}MnN_3O5^+$ (below).

## III. NMR Studies

### a. DOSY analysis

Diffusion experiments were performed using the bipolar pulse longitudinal eddy current delay pulse sequence (pulse program ledbpgp2s in the Bruker library). Sine shaped pulse field gradient were used with a length $\delta$ of 3 ms and the gradient intensity was linearly incremented from 0.96 to 47.19 G $cm^{-1}$ over 20 experiments and 50 ms were used for the diffusion time Δ. Data were processed with MNova. The phase and baseline of each proton spectrum were carefully corrected. All data were processed using Mnova software using the "peak heights" fit. Diffusion curves were then fitted using exponential decay equation model Exp2PMod1 from Origin, which match the results obtained when using MNova software mono-exponential fit (Figure S12). Bayesian transformation from MNova software was used to obtain DOSY spectra represented in Figure S13 presented with chemical shifts (ppm) on the horizontal axis and diffusion coefficients on the vertical axis ($cm^2 \cdot s^{-1}$).

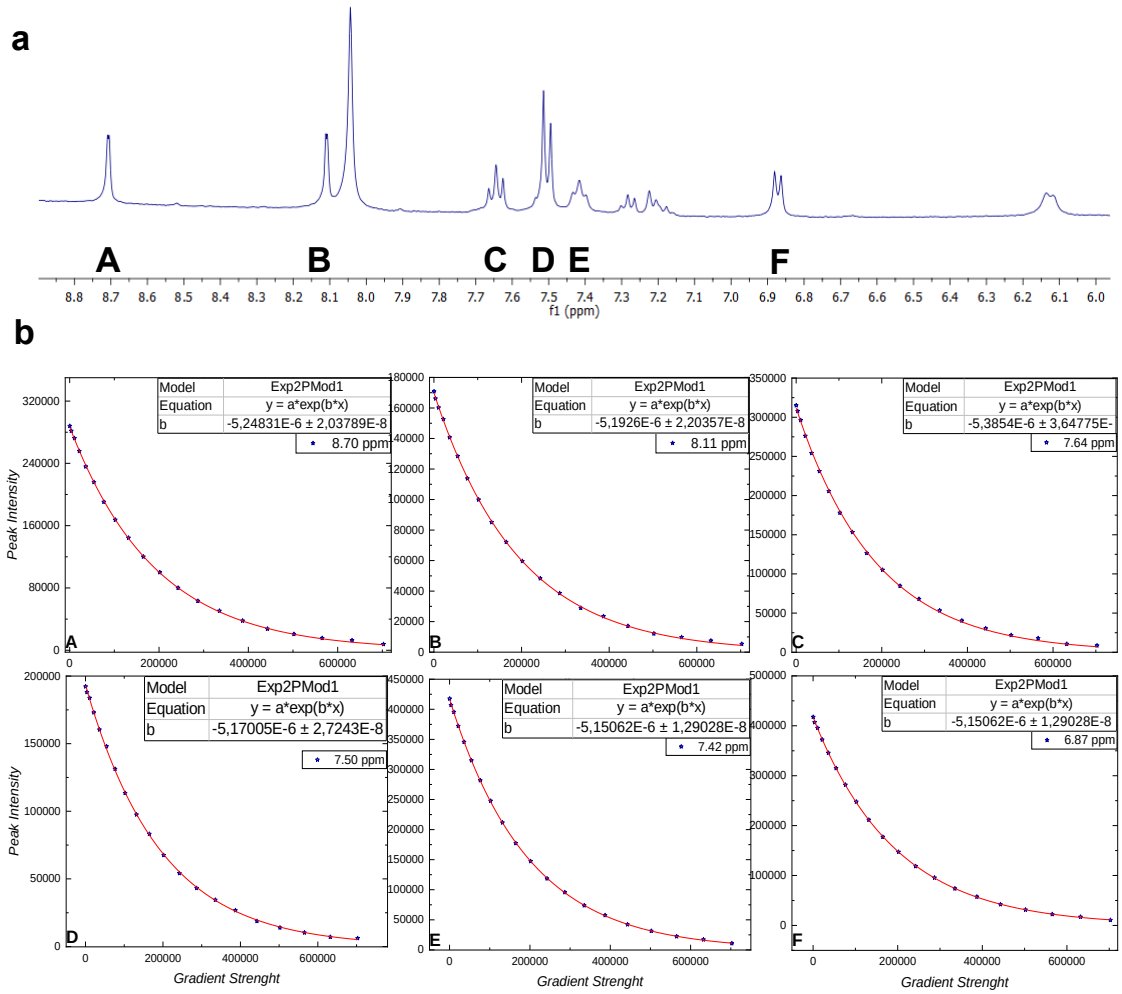


**Figure S12**. **a,** Region of the $^{1}$H NMR spectrum displaying the signals of interest for diffusion measurements; **b**, decaying curves obtained for the different signals recorded for complex **1** (5 mM) in 0.1 M TBAH DMF-$d_7$ solution are shown together with the best fit to a mono exponential decay.

$$I = I_0 \cdot e^{-D \cdot x} \qquad \text{(eq. 1)}$$

$$x = \gamma^2 \cdot g^2 \cdot \delta^2 \cdot \left(\Delta - {}^{\delta}/_{3}\right) \qquad \text{(eq. 2)}$$

I = peak intensity; $I_0$ = max. peak intensity; D = diffusion coefficient; δ = gradient duration; g = gradient strength; γ = gyromagnetic ration; Δ = echo delay.

$$D = 534 \cdot 10^{-12} \pm 2 \cdot 10^{-12}\ m^2 \cdot s^{-1}$$

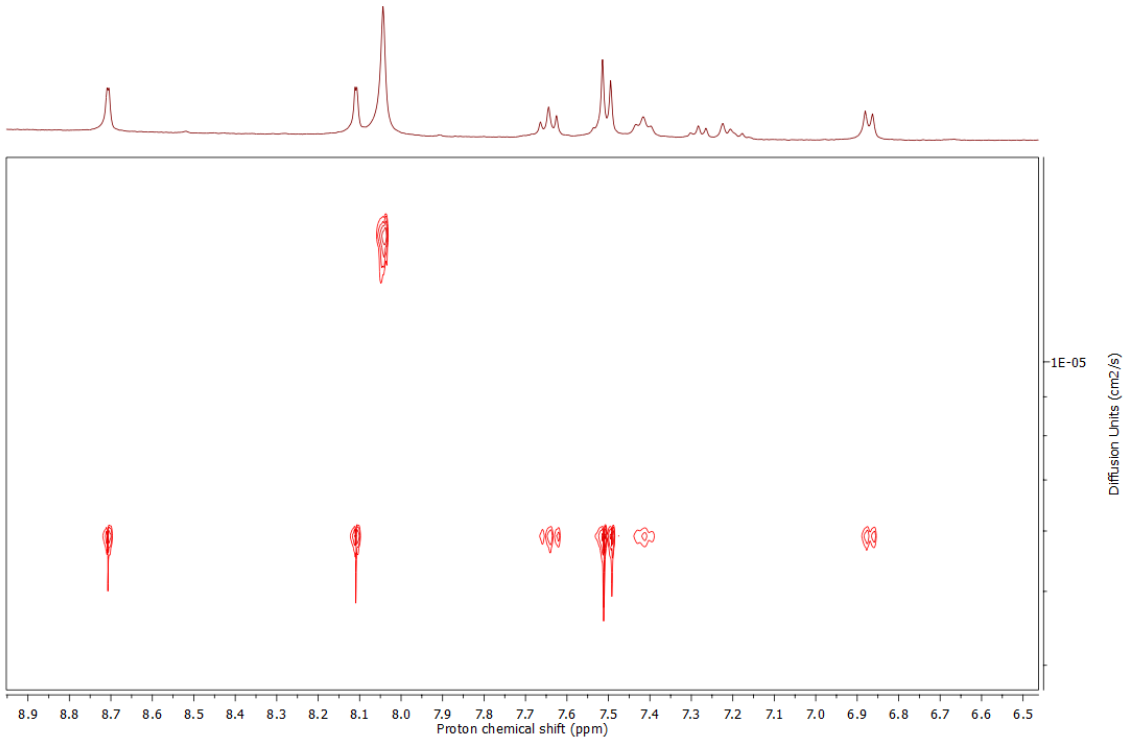


**Figure S13**. DOSY map computed from the diffusion data recorded at 400 MHz on the Complex **1** (5 mM) in a 0.1 M TBAH DMF-$d_7$ solution.

### b. NMR analysis of consecutive addition of [K][B($Ar^F$)$_4$] to 1 in DMF-$d_7$

Sample Preparation: Inside the glovebox, K[B($Ar^F$)$_4$] ($Ar^F$ is 3,5-bis(trifluoromethyl)phenyl) was added consecutively to a Teflon capped NMR tube containing complex **1** (6 mM) in 0.6 mL of 0.1M TBAH, DMF-$d_7$ solution and mesitylene as internal standard. We established the aromatic mesitylene signal, present in solution, as a reference (6.98 ppm) to evaluate the chemical shift evolution from complex **1**. As the concentration of K[B($Ar^F$)$_4$] increases in the solution, most of the proton signals experienced downfield shift with respect to their initial chemical shift values.

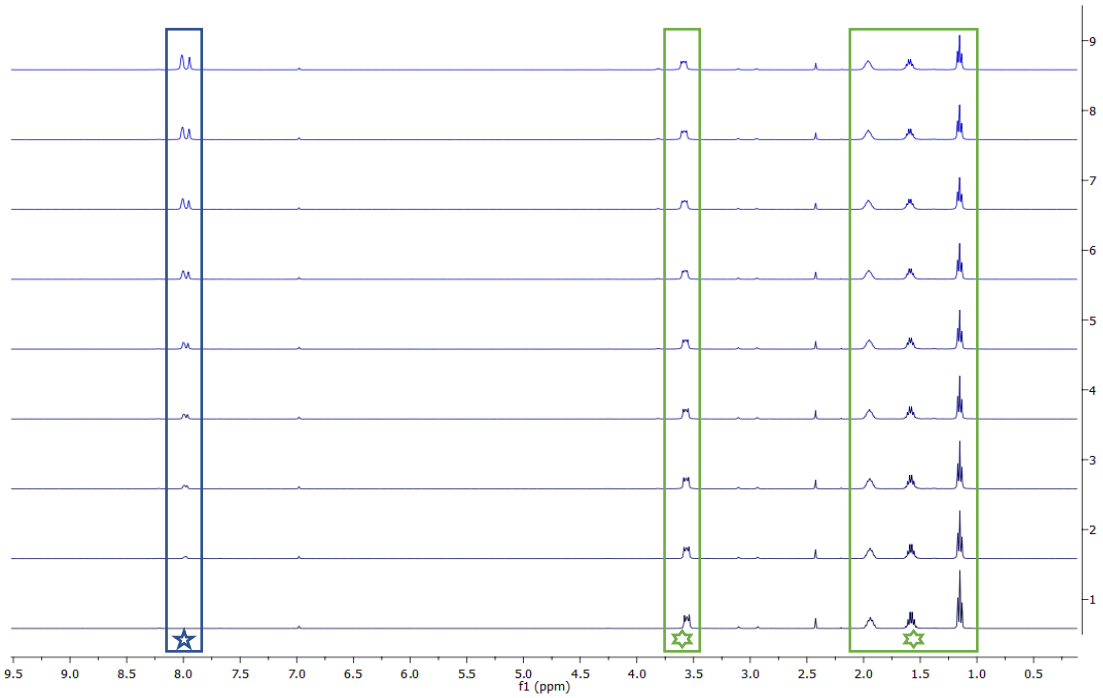


**Figure S14**. $^{1}$H NMR spectra recorded in a 400 MHz of **1** (6 mM) in 0.5 mL DFM-$d_7$ solution at 20 °C containing 0.1 M of TBAH with subsequent additions of K[B(Ar$^{F}$)$_4$]. Blue Star, K[B(Ar$^{F}$)$_4$]; green star, TBAH. Singlet at 2.4 ppm belongs to the methyl groups from the internal standard, mesitylene.

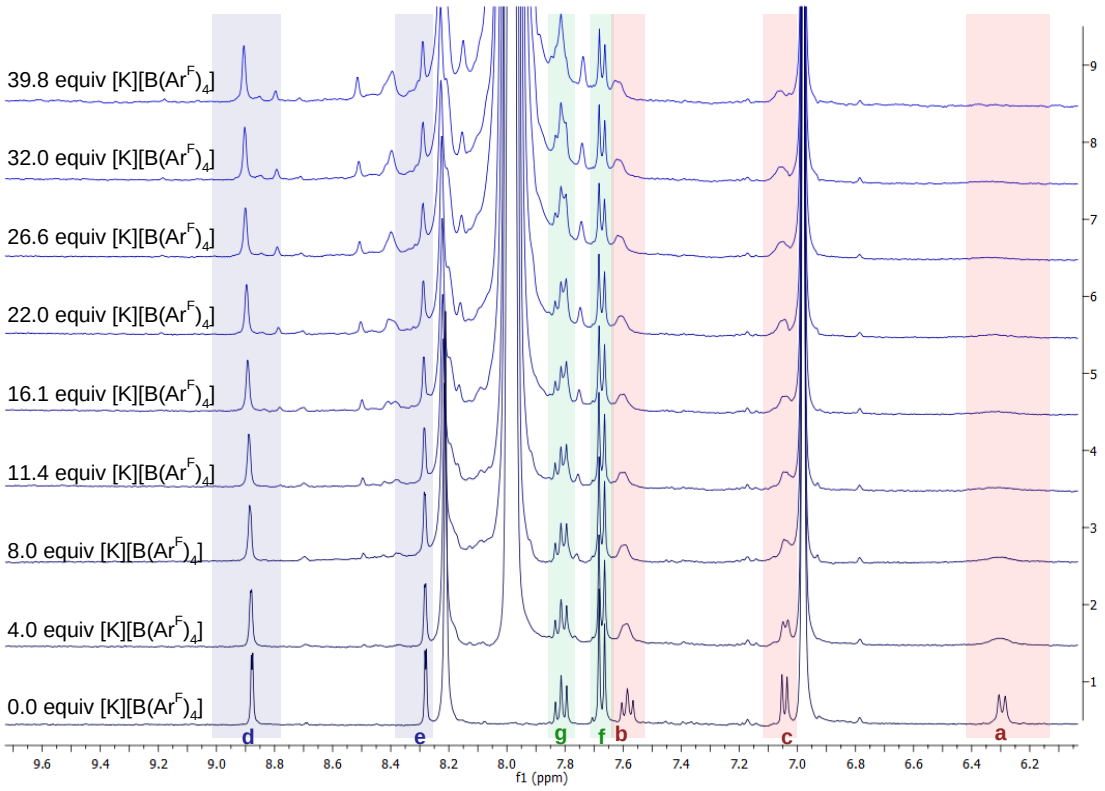


**Figure S15**. Zoomed $^1$H NMR spectra recorded at 400 MHz of **1** (6 mM) in 0.5 mL DFM-$d_7$ solution at 20 °C containing 0.1 M of TBAH with subsequent additions of K[B(Ar$^F$)$_4$]. Singlet at 6.98 ppm belongs to the aromatic protons from the internal standard, mesitylene.

The signals experiencing a larger shift in their chemical resonance correspond to those protons located at the pyridone-ring, followed by protons located at the NHC-backbone. The protons located at the diip-substituent show negligent shifts. The evolution of chemical shift values for the different H-signals is depicted in Fig. S16 representing the difference in chemical shift (Δδ) versus equivalents of K[B(Ar$^F$)$_4$] added.

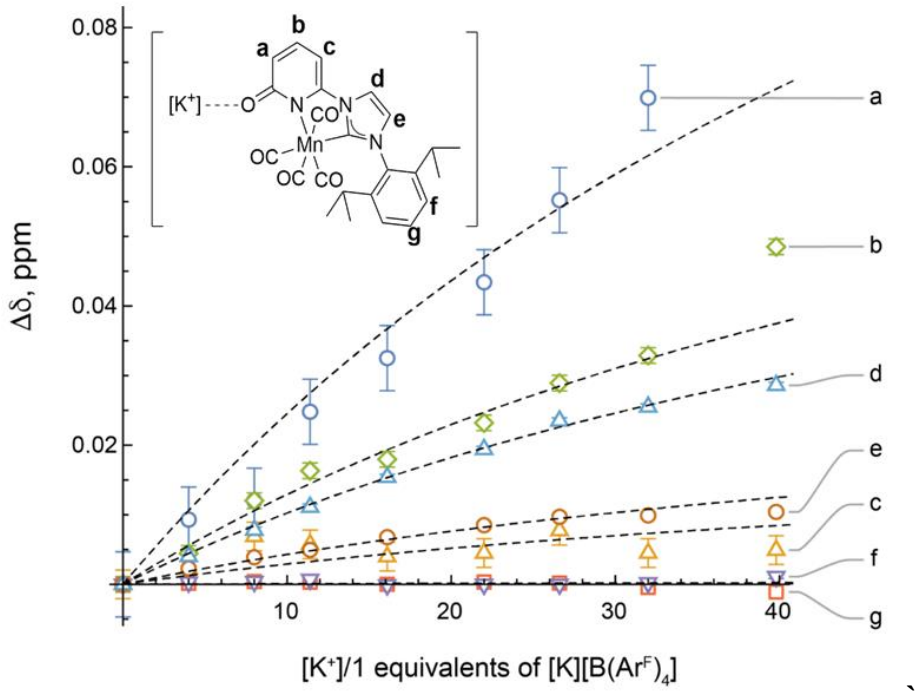


**Figure S16**. The set of chemical shift titration curves that were obtained from the addition of K[B(Ar$^F$)$_4$] to **1** (6 mM) in 0.6 mL DFM-$d_7$ solution at 20 °C containing 0.1 M TBAH. Dashed curves represent the best fits modelling the interaction process between **1** and the alkali salt. The details of the fitting protocol are given in Table S1.

**Table S1**. Parameters of the best fits determined for the chemical shift titration curves shown in Figure S16.

| **K[B(Ar$^F$)$_4$]**<br>**$K_d$ = 0.4 ± 0.2 Mol·L$^{-1}$** | | |
|---|---|---|
| **Proton Label** | **$\delta_{bound}$** | **Standard deviation** |
| ***a*** | 6.49 ppm | 0.05 ppm |
| ***b*** | 7.69 ppm | 0.02 ppm |
| ***c*** | 7.06 ppm | 0.01 ppm |
| ***d*** | 8.96 ppm | 0.02 ppm |
| ***e*** | 8.31 ppm | 0.01 ppm |
| ***f*** | 7.813 ppm | 0.001 ppm |
| ***g*** | 7.674 ppm | 0.001 ppm |

The interaction between **1** and each alkali salt was modelled by a 1:1 equilibrium undergoing a fast exchange process:[1]

$$\mathbf{1} + [\mathrm{K}][\mathrm{B}(\mathrm{Ar}^{F})_4] = \mathbf{1}\cdots\mathrm{K}^{+}, [\mathrm{B}(\mathrm{Ar}^{F})_4]^{-} \quad \text{(S1)}$$

The fast exchange regime leads to the observation of an average chemical shift under our experimental conditions. The parameters of this interaction model that were adjusted are the affinity constant ($K_d$) of the equilibrium, and the chemical shift of each proton site in its bound form ($\delta_{bound}$). The fits were performed using a least squares method. The experimental point corresponding to 39.8 equivalents was discarded to improve the quality of the fit. The fit was performed as follows: the titration curves of proton sites *b*, *d*, and *e*, which were found to provide the most reliable shift values for $K[B(Ar^F)_4]$, were fitted together to determine the value of the affinity constant. For proton sites *a*, *c*, *f* and *g*, only $\delta_{bound}$ was adjusted, using the value of $K_d$ determined on other proton sites as a constant. Overall, we note that the weak chemical shift variation that is observed for the NMR titration curve has led to a rather low accuracy in the determination of the affinity constant.[2]

## IV. IR-spectroscopic studies in the presence of alkali metals salts

The Greek symbols α, β, χ and δ, highlight the changes in the IR-spectra due to the incremental addition of the corresponding $M(ClO_4)_n$ salt (M = Li, K, Na or Mg) in 0.1 M TBAH solution of DMF (Fig. S17-S20). Therefore, the changes in the different CO bands are not due to the interaction of $M^{n+}$ with complex **1** but the overlap bands of complex **1** and those resulting from adding the corresponding perchlorate salt.

### a. Addition of $LiClO_4$

Procedure: To 3 mL solution of complex **1** (1mM) containing 0.1 M of TBAH in dry DMF, $LiClO_4$ was added consecutively under Ar.

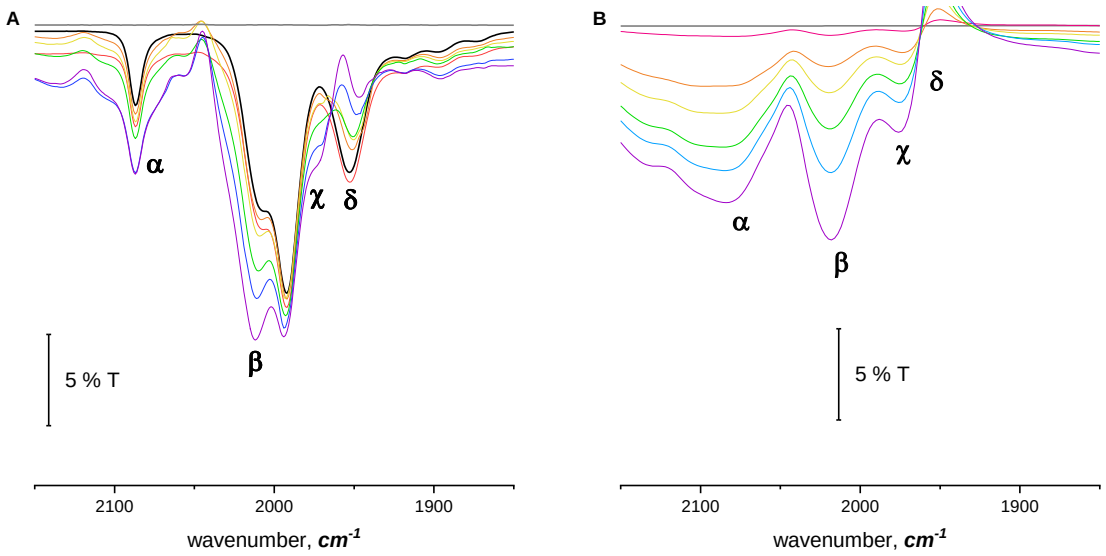


**Figure S17**. **A**, Solution IR data for a DMF solution containing 1mM of **1** in the presence of 0.1 M of TBAH with consecutive additions of $LiClO_4$ (blank (grey), No $LiClO_4$ added (black), 5 mM (red), 17 mM (orange), 35 mM (yellow), 68 mM (green), 102 mM (blue), and 155 mM (purple)). **B**, Solution IR data for 0.1 M of TBAH, DMF solution with consecutive additions of $LiClO_4$ (blank (grey), 8 mM (red), 23 M (orange), 45 mM (yellow), 79 mM (green), 121 mM (blue), and 192 mM (purple)).

### b. Addition of $NaClO_4$

Procedure: To a 3 mL solution of complex **1** (1mM) containing 0.1 M of TBAH in dry DMF, $NaClO_4$ was added consecutively under Ar.

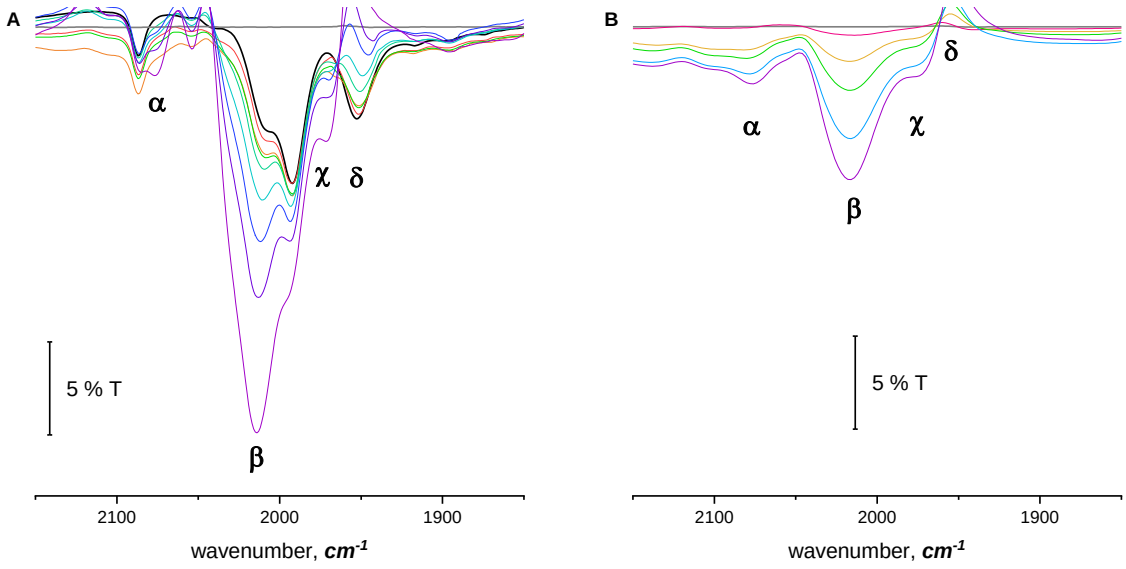


**Figure S18**. Solution IR data for a DMF solution containing 1mM of **1** in the presence of 0.1 M of TBAH with consecutive additions of $NaClO_4$ (blank (grey), No $NaClO_4$ added (black), 5 mM (red), 14 mM (orange), 26 mM (yellow), 50 mM (green), 86 mM (turquoise), 138 mM (blue), 191 mM (violet), and 352 mM (purple). **B**, Solution IR data for 0.1 M of TBAH, DMF solution with consecutive additions of $NaClO_4$ (blank (grey), 8 mM (red), 27 mM (orange), 54 mM (green), 96 mM (blue) and 145 mM (purple)).

### b. Addition of $KClO_4$

Procedure: To a 3 mL solution of complex **1** (1mM) containing 0.1 M of TBAH in dry DMF, $KClO_4$ was added consecutively under Ar.

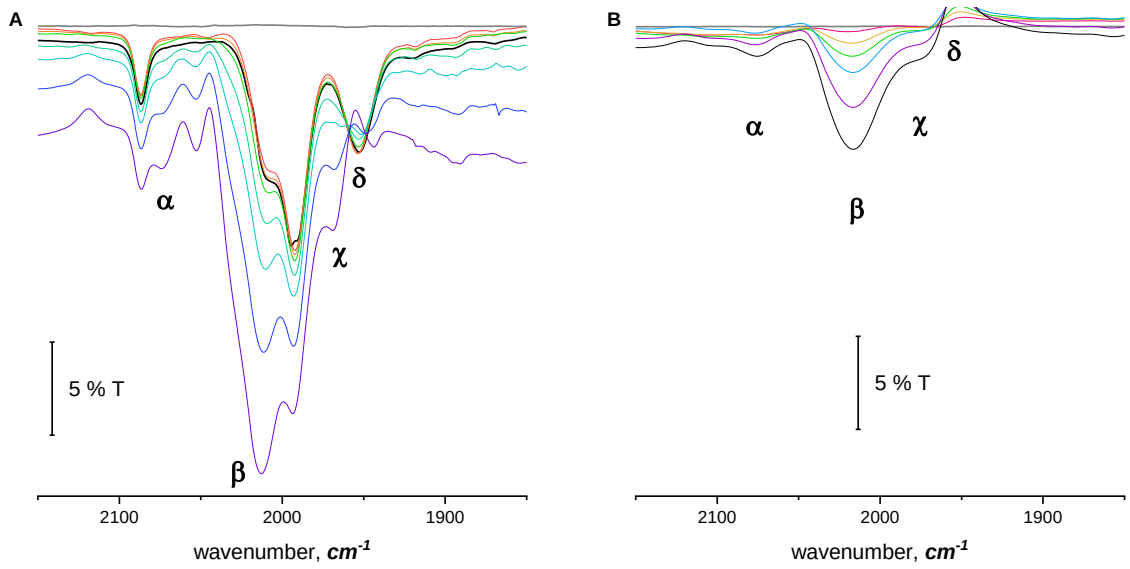


**Figure S19**. **A**, Solution IR data for a DMF solution containing 1mM of **1** in the presence of 0.1 M of TBAH with consecutive additions of $KClO_4$ (blank (grey), No $KClO_4$ added (black), 4.0 mM (red), 9 mM (orange), 26 mM (light green), 52 mM (green), 93 mM (turquoise), 168 mM (blue) and 290 mM (purple)). **B**, Solution IR data for 0.1 M of TBAH, DMF solution with consecutive additions of $KClO_4$ (blank (grey), 5 mM (red), 17 mM (orange), 30 mM (green), 50 mM (blue), 79 mM (purple) and 118 mM (black)).

### c. Addition of $Mg(ClO_4)_2$

Procedure: To a 3 mL solution of complex **1** (1mM) containing 0.1 M of TBAH in dry DMF, $Mg(ClO_4)_2$ was added consecutively under Ar.

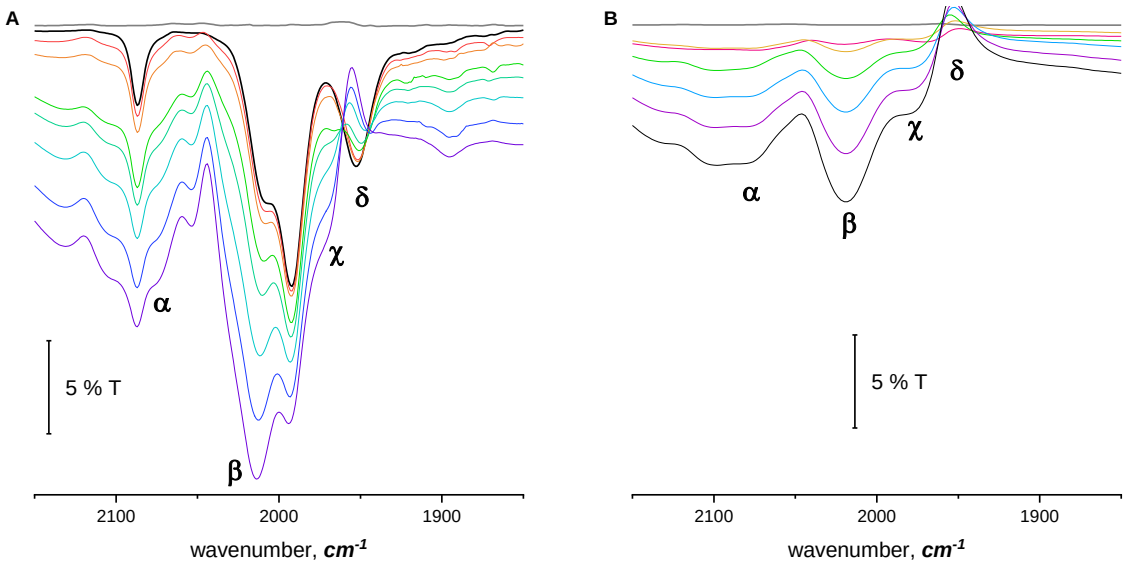


**Figure S20**. Solution IR data for a DMF solution containing 1mM of **1** in the presence of 0.1 M of TBAH with consecutive additions of $Mg(ClO_4)_2$ (blank (grey), No $Mg(ClO_4)_2$ added (black), 3 mM (red), 6 mM (orange), 18 mM (light green), 37 mM (green), 74 mM (turquoise), 105 mM (blue) and 139 mM (purple)). **B**, Solution IR data for 0.1 M of TBAH, DMF solution with consecutive additions of $Mg(ClO_4)_2$ (blank (grey), 3 mM (red), 9 mM (orange), 19 mM (green), 34 mM (blue), 52 mM (purple) and 74 mM (black)).

**d. Solution IR after bulk electrolysis**.

The bulk electrolysis was performed on 3mM solution of **1** in DMF with 0.1 M TBAH at an applied potential of –1.9 V for 3 hours under $CO_2$. After electrolysis experiment, the solution was spared with Ar for 30 mins to displace the $CO_2$ dissolved. Later, the IR cell was filled with the electrolysis solution (*ca*. 0.1 mL) and the spectrum was recorded. Blank solution with 0.1 M TBAH was used to obtain base-line spectra.

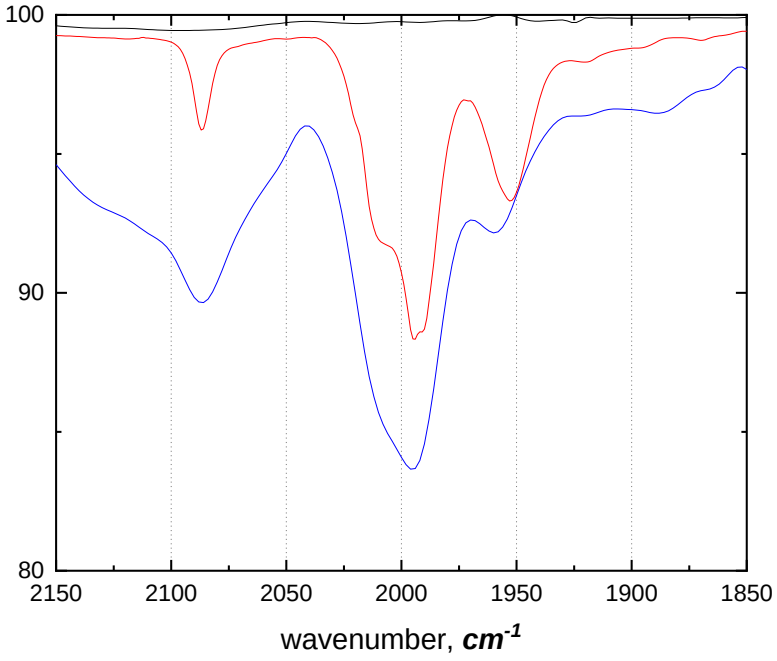


**Figure S21**. Solution IR data for a DMF solution containing: 0.1 M of TBAH (black line); 0.1 M of TBAH, 1 mM of **1** (red line); 0.1 M of TBAH, 3 mM of **1** after bulk electrolysis (blue line).

**e. Solution IR after bulk electrolysis in the presence of 45 mM of $KClO_4$.**

The bulk electrolysis was performed on 3mM solution of **1** in DMF with 0.1 M TBAH and 45mM $KClO_4$ at an applied potential of –1.8 V for 2 hours under $CO_2$. After electrolysis experiment, the solution was spared with Ar for 30 mins to displace the $CO_2$ dissolved. Later the IR cell was filled with the electrolysis solution (*ca*. 0.1 mL) and the spectrum was recorded. Blank solution with 0.1 M TBAH was used to obtain base-line spectra.

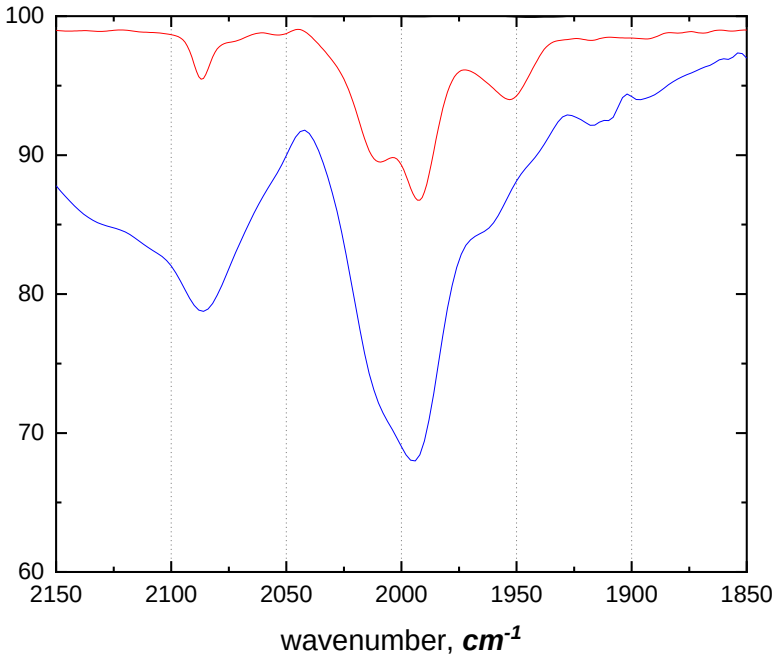


**Figure S22**. Solution IR data for a DMF solution containing: 0.1 M of TBAH (black line); 0.1 M of TBAH, 1 mM of **1** and 51.6 mM of $KClO_4$ (red line); 0.1 M of TBAH, 3 mM of **1** and 45 mM of $KClO_4$ after bulk electrolysis (blue line).

## V. Electrochemical Studies

**Cyclic voltammetry (CV) measurements**. All the electrochemical measurements were performed in a water jacketed electrochemical cell at 20 °C. The solution was prepared inside the glovebox working station under $N_2$ and purged with Ar or $CO_2$ for 15 mins before cyclic voltammograms were recorded. Ohmic drop was compensated using the positive feedback compensation implemented in the instrument between successive measurements.

*Experiments using Lewis acid (perchlorate salts of $Li^+$, $K^+$, $Na^+$, and $Mg^{2+}$).* Inside the glovebox, different amounts of the corresponding Lewis acids were placed into 3 mL vials. Later, each vial was sealed with a rubber septa and Teflon tape and removed from the glovebox. Once outside, 2 mL of solution from the electrochemical cell were added to generate different desire concentrations (5mM, 10 mM, 45 mM, 90 mM, 180 mM, and 360 mM). Sonication was performed for 1 min to completely dissolve the alkali salt. The resulting solution was injected back into the cell under Ar. The solutions were additionally purged with Ar or $CO_2$ for 10 mins after the addition of Lewis acid and CVs were recorded. For each concentration, the CV measurements were repeated at least twice to ensure the reproducibility.

**a. Electrochemical characterization**

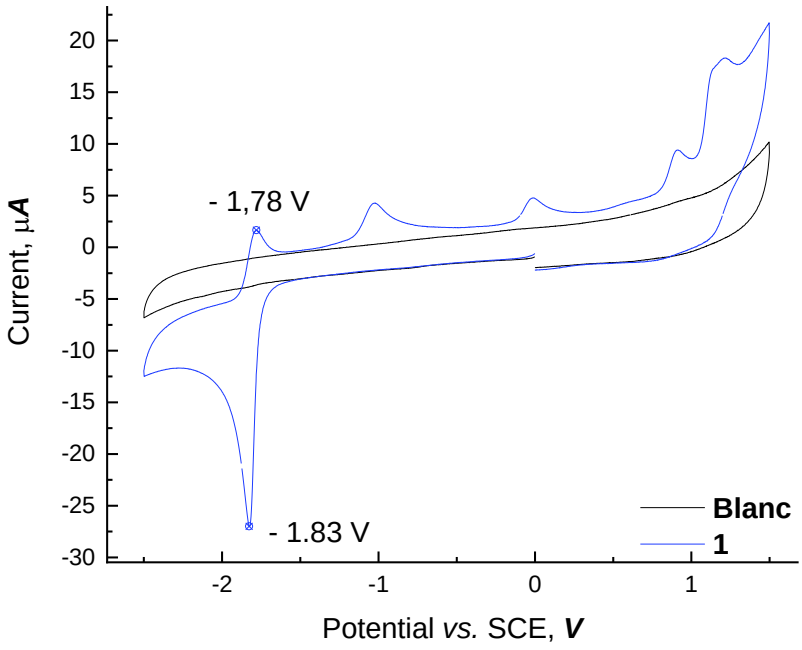


**Figure S23.** Comparison of CV of complex **1** and blank solution. Conditions: Anhydrous DMF, 0.1 M TBAH, **1** (1mM), 20 ºC under Ar, 100 $mV \cdot s^{-1}$.

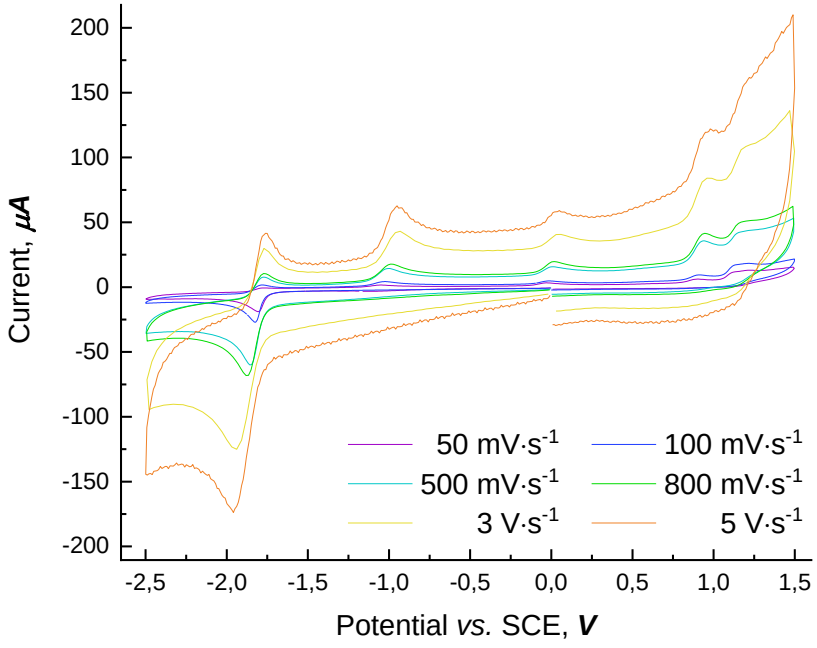


**Figure S24.** Comparison of CVs of complex **1** recorded at different Scan Rates. Conditions: Anhydrous DMF, 0.1 M TBAH, **1** (1mM), 20 ºC under Ar.

Standard reduction potential $Mn^{I} \rightarrow Mn^{0}$, $E^{0} = -1.814$ (V vs. SCE).

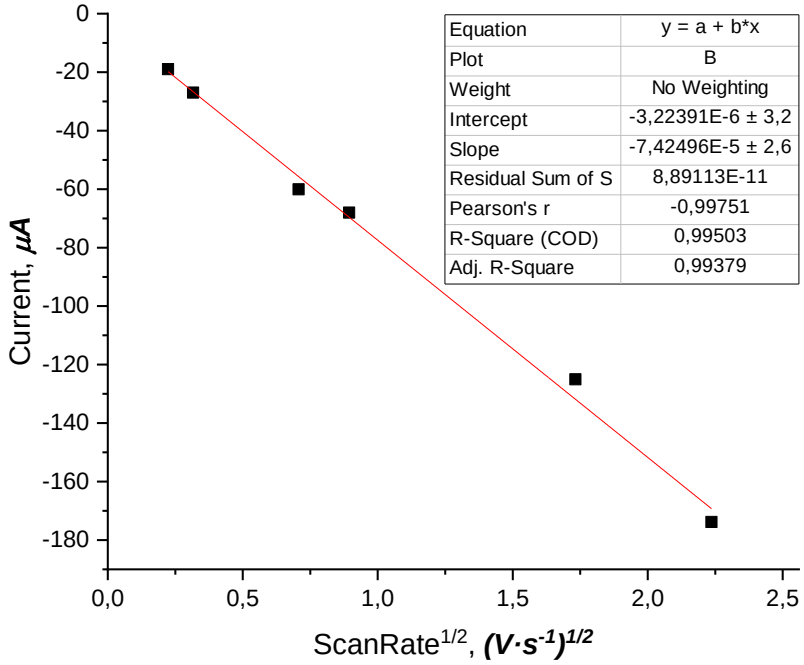


**Figure S25.** Plot of maximum current for the major reductive peak versus the square root of the scan rate for scan rates of 0.05, 0.10, 0.50, 0.80, 3.0 and 5.0 $V \cdot s^{-1}$.

Conditions: Anhydrous DMF, 0.1 M TBAH, **1** (1mM), 20 ºC under Ar.

- **Randles-Sevcik equation**

The Randles-Sevcik equation (eq. 3), which describes the effect of scan rate on the peak current was applied to obtain the number of electrons.

$$i_p = 0.4463 \cdot n \cdot F \cdot C \cdot \sqrt{n \cdot F \cdot D / R \cdot T} \cdot \sqrt{v} \qquad \text{(eq. 3)}$$

$i_p$ = current maximum (A); $n$ = number of electrons transferred; A = electrode area ($cm^2$); $F$ = Faraday constant ($C \cdot mol^{-1}$); $D$ = diffusion coefficient ($cm^2 \cdot s^{-1}$); $C$ = concentration ($mol \cdot cm^{-3}$); $v$ = scan rate in ($V \cdot s^{-1}$); $R$ = Gas constant ($J \cdot K^{-1} \cdot mol^{-1}$) ; $T$ = temperature (K).

We used the data from Figure S27 and represented in Figure S28 to arrange equation 3 as shown below:

$$n = \sqrt[3]{\frac{R \cdot T}{F D} \cdot \left(\frac{slope}{0.4463 \cdot F \cdot A \cdot C}\right)^2} \qquad \text{(eq. 4)}$$

Slope = $7.424 \cdot 10^{-5}$; A = 0.0707 ($cm^2$); $F$ = 96845 ($C \cdot mol^{-1}$); $D$ = $534 \cdot 10^{-8}$ ($cm^2 \cdot s^{-1}$); $C$ = $1.02 \cdot 10^{-6}$ ($mol \cdot cm^{-3}$); $R$ = 8.3145 ($J \cdot K^{-1} \cdot mol^{-1}$) ; $T$ = 294.15 (K).

With the experimental values shown, we deduced n = 1.39.

Since the value was off by 0.39 from the expected 1 electron value. We performed the CV measurement of complex **1** (red line, Figure S29) in the presence of 1 equivalent of ferrocene (blue line, Figure S29). Comparison of the corresponding reductive areas for complex **1** ($V_{ini}$= – 1.57 V, $V_{fin}$ = – 2.23 V) and ferrocene ($V_{ini}$= 0.05 V, $V_{fin}$ = 0.59 V) gave as a value of n = 0.875 (Figure S30 and Table S2).

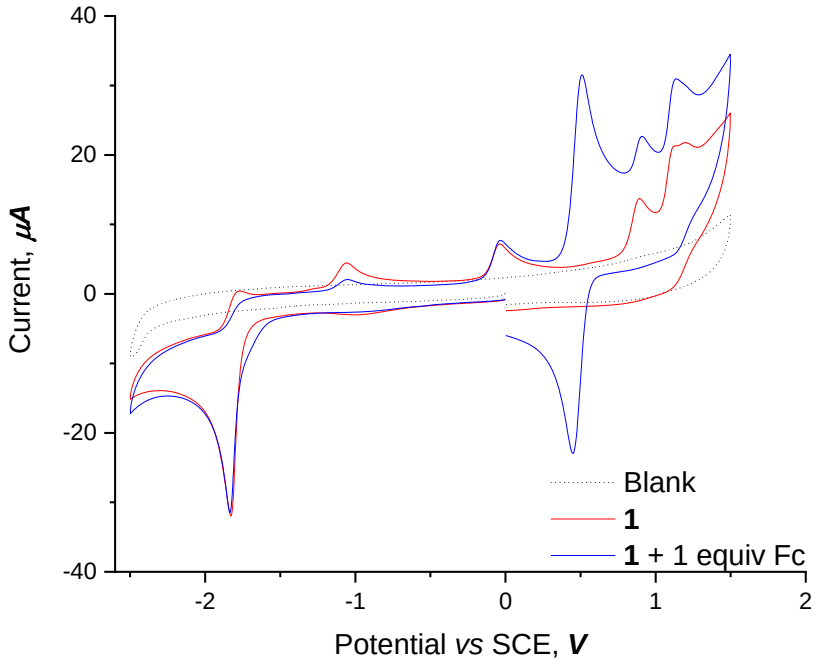

**Figure S26.** CV comparisons of blank (dotted line), complex **1** (red line) and complex **1** in the presence of 1 equivalent of ferrocene (blue line) recorded at 0.1 $V \cdot s^{-1}$ in anhydrous DMF, 0.1 M TBAH, **1** (1mM), 20 ºC under Ar.

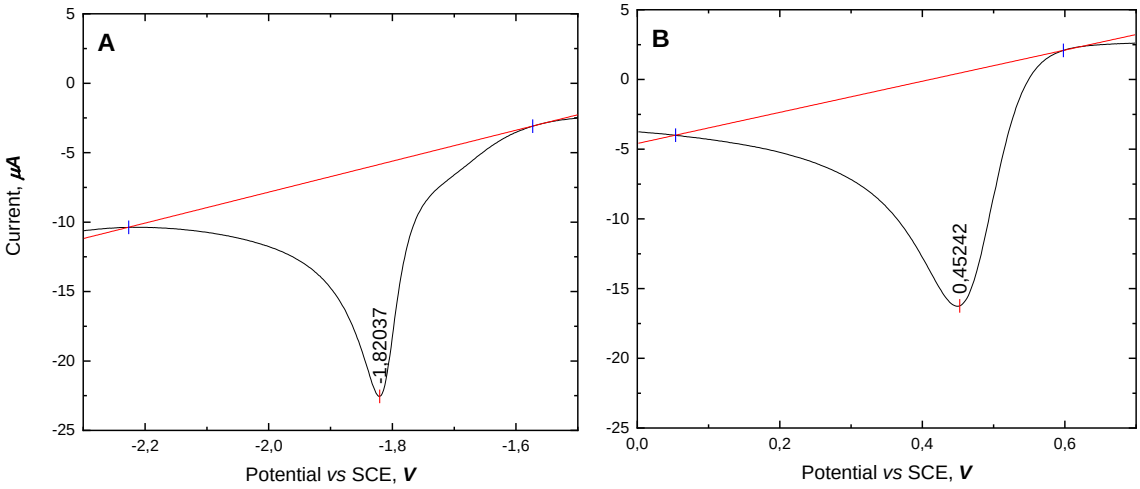


**Figure S27.** Integration area for reductions events of $Mn^{I} \rightarrow Mn^{0}$ (**A**) and $Fc \rightarrow Fc^{+}$ (**B**) using spectrum recorded for complex **1** in the presence of 1 equivalent of ferrocene (blue line, Figure S29) recorded at 0.1 $V \cdot s^{-1}$ in anhydrous DMF, 0.1 M TBAH, **1** (1mM), 20 ºC under Ar.

**Table S2**. Table with values obtained from calculating the area from curves **A** and **B** from Figure S30.

| Peak | Area | $V_{ini}$ (V) | $V_{fin}$ (V) | $V_{max}$ (V) | $I_{max}$ (µA) |
|---|---|---|---|---|---|
| **A** | $-2.80 \cdot 10^{-6}$ | -2.227 | -1.573 | -1.820 | -16.7 |
| **B** | $-3.21 \cdot 10^{-6}$ | 0.053 | 0.598 | 0.452 | -16.7 |

$$n = \frac{Area_A}{Area_B} = 0.875$$

**b. Electrochemical studies under $CO_2$**

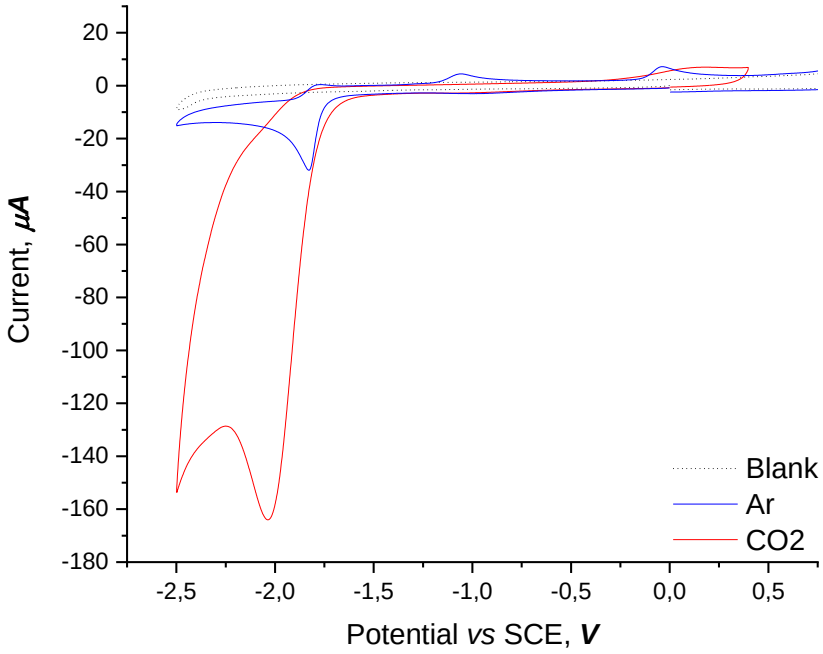


**Figure S28.** CV comparison of blanc and complex **1** under Ar and $CO_2$. Conditions: Anhydrous DMF, 0.1 M TBAH, **1** (1mM), 20 ºC, 100 $mV \cdot s^{-1}$.

### c. Effects of Lewis acids

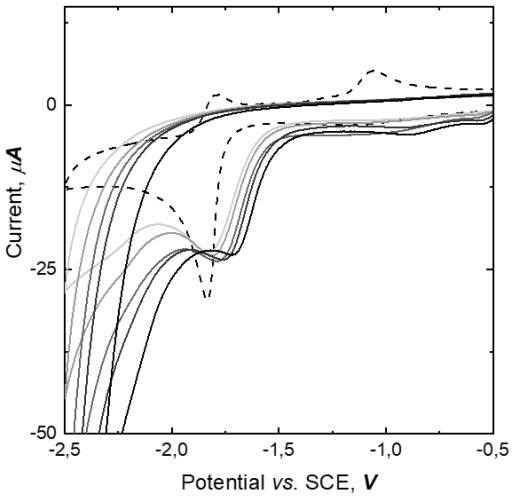


**Figure S29.** CVs of complex **1** in the presence of different concentrations of $Mg(ClO_4)_2$. Conditions: Anhydrous DMF, 0.1 M TBAH, **1** (1mM), 20 ºC under Ar. No $Mg(ClO_4)_2$ added (dashed line). Concentrations from lighter to darker color: 5, 10, 45, 90 and 180 mM.

From the CVs analysis it can be observed that when 90 mM or higher concentrations of $Mg(ClO_4)_2$ was present in solution, dramatic increase in current was observed. We speculate that this current enhancement is likely due to reductive processes from DMF by the glassy carbon electrode favored by the presence of $Mg^{2+}$ in solution.

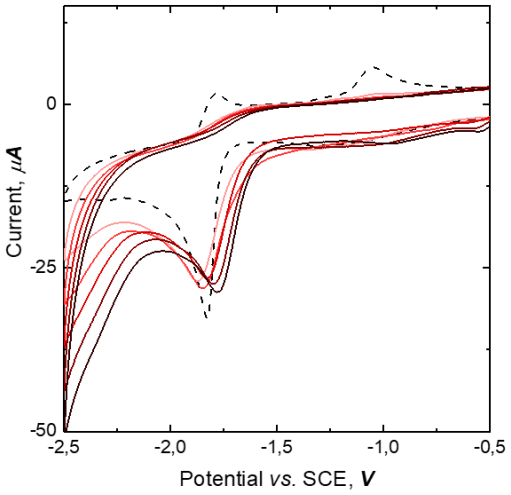


**Figure S30.** CVs of complex **1** in the presence of different concentrations of $LiClO_4$. Conditions: Anhydrous DMF, 0.1 M TBAH, **1** (1mM), 20 ºC under Ar. No $LiClO_4$ added (dashed line).

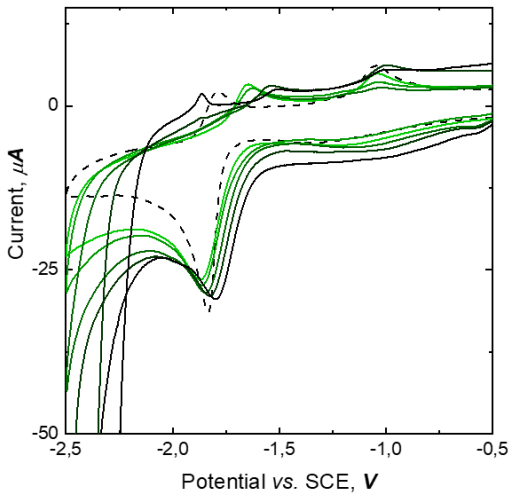


**Figure S31.** CVs of complex **1** in the presence of different concentrations of $NaClO_4$. Conditions: Anhydrous DMF, 0.1 M TBAH, **1** (1mM), 20 ºC under Ar. No $NaClO_4$

added (dashed line). Concentrations from lighter to darker color: 5, 10, 45, 90, 180 and 360 mM.

From the CVs analysis it can be observed that when 90 mM or higher concentrations of $NaClO_4$ was present in solution, dramatic increase in current was observed. We speculate that this current enhancement is likely due to reductive processes from DMF by the glassy carbon electrode favored by the presence of $Na^+$ in solution.

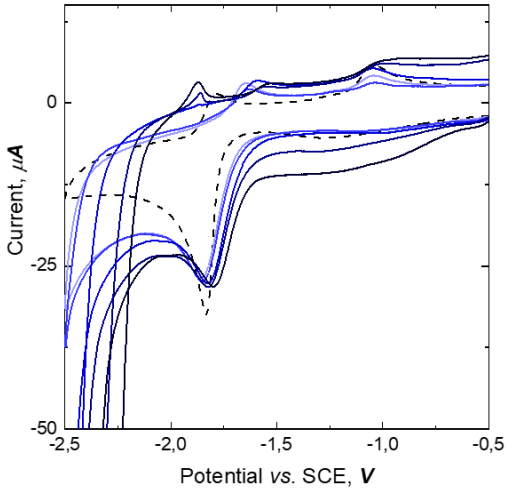


**Figure S32.** CVs of complex **1** in the presence of different concentrations of $KClO_4$. Conditions: Anhydrous DMF, 0.1 M TBAH, **1** (1mM), 20 ºC under Ar. No $KClO_4$ added (dashed line). Concentrations from lighter to darker color: 5, 10, 45, 90, 180 and 360 mM.

From the CVs analysis it can be observed that when 45 mM or higher concentrations of $KClO_4$ was present in solution, dramatic increase in current was observed. We speculate

that this dramatic current enhancement is likely due reductive processes from DMF by the glassy carbon electrode favored by the presence of $K^+$ in solution.

- **Nernstian response from adding different alkali salts to 1 under Ar**

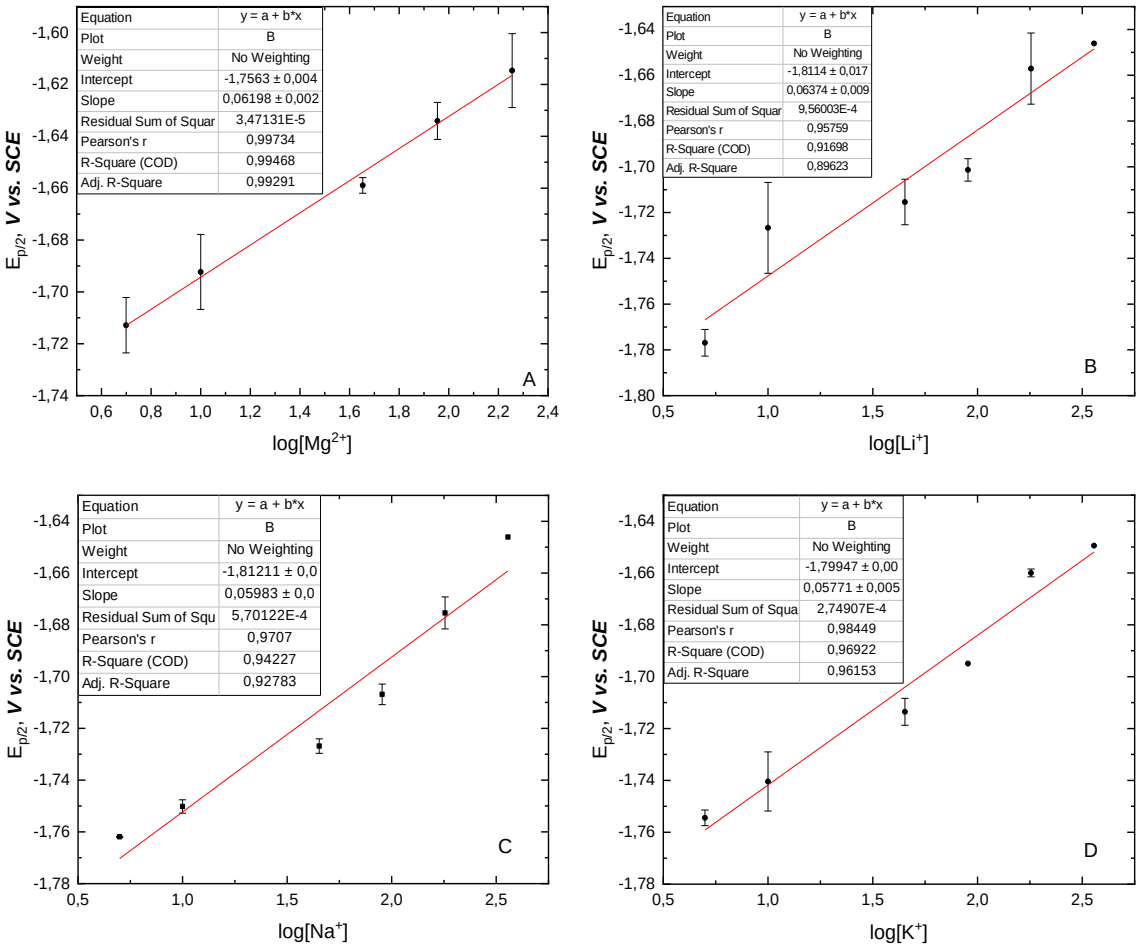


**Figure S33**. Plots of $E_{p/2}$ (V *vs.* SCE) against the Log[$M^{n+}$] for the different alkali salt additions (**A**, $Mg^{2+}$; **B**, $Li^+$; **C**, $Na^+$; **D**, $K^+$). The set of $E_{p/2}$ were obtained from the addition of $M(ClO_4)_n$ to **1** (1 mM) in 6 mL DMF solution at 20 °C containing 0.1 M TBAH. Red line represents the linear fit modelling.

**Table S3**. Relevant information from linear fitting at the different plots represented in Figure S33.

| Plot | $[M^{n+}]$ | $R^2$ | Slope | Intercept |
|---|---|---|---|---|
| **A** | $[Mg^{2+}]$ | 0.995 | 0.062 | -1.756 |
| **B** | $[Li^{+}]$ | 0.917 | 0.064 | -1.811 |
| **C** | $[Na^{+}]$ | 0.942 | 0.059 | -1.812 |
| **D** | $[K^{+}]$ | 0.969 | 0.058 | -1.799 |

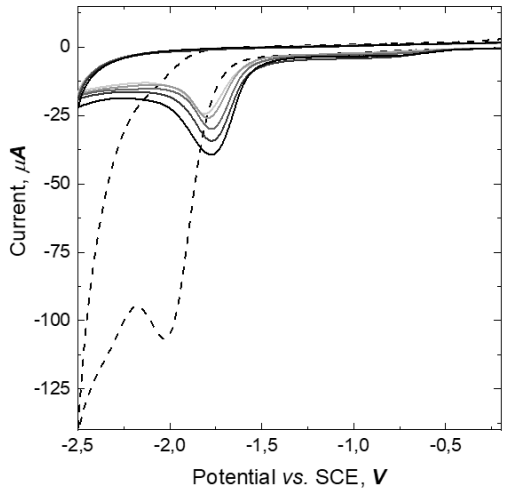


**Figure S34.** CVs of complex **1** in the presence of different concentrations of $Mg(ClO_4)_2$. Conditions: Anhydrous DMF, 0.1 M TBAH, **1** (1mM), 20 ºC under $CO_2$. No $Mg(ClO_4)_2$ added (dashed line). Concentrations from lighter to darker color: 5, 10, 45, 90, and 180 mM.

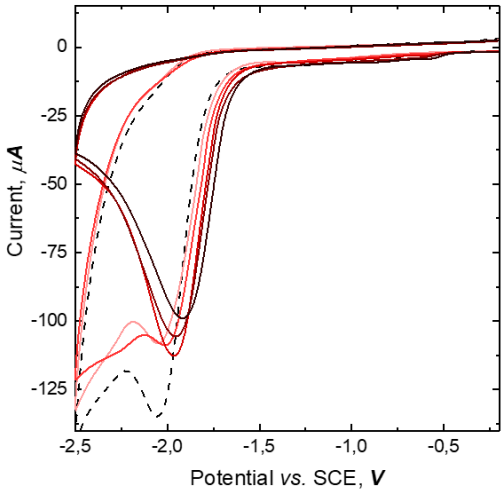


**Figure S35.** CVs of complex **1** in the presence of different concentrations of $LiClO_4$. Conditions: Anhydrous DMF, 0.1 M TBAH, **1** (1mM), 20 ºC under $CO_2$. No $LiClO_4$ added (dashed line). Concentrations from lighter to darker color: 5, 10, 45, 90, 180 and 360 mM.

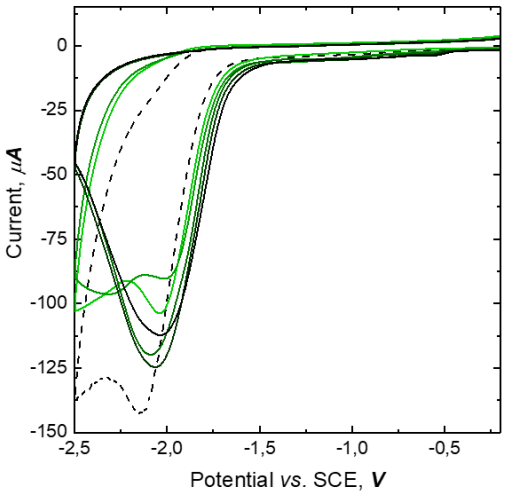


**Figure S36.** CVs of complex **1** in the presence of different concentrations of $NaClO_4$. Conditions: Anhydrous DMF, 0.1 M TBAH, **1** (1mM), 20 ºC under $CO_2$. No $NaClO_4$

added (dashed line). Concentrations from lighter to darker color: 5, 10, 45, 90, 180 and 360 mM.

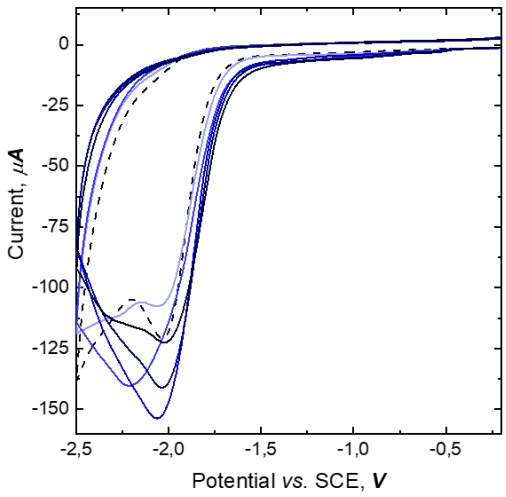


**Figure S37.** CVs of complex **1** in the presence of different concentrations of $KClO_4$. Conditions: Anhydrous DMF, 0.1 M TBAH, **1** (1mM), 20 ºC under $CO_2$. No $KClO_4$ added (dashed line). Concentrations from lighter to darker color: 5, 10, 45, 90, 180 and 360 mM.

**Bulk Electrolysis.** Bulk electrolysis experiments were carried out in PARSTAT 4000 potentiostat using a pear shaped four-neck electrochemical cell. The set-up consists of a glassy carbon plate working electrode, a Pt mesh counter electrode, separated from the solution by a porous glass frit and a SCE reference electrode. Prior to the electrolysis, the working electrode was polished with diamond paste (0.25 μm particle size) and rinsed and sonicated in acetone and Milli-Q water and dried before use. The bulk reductions were carried out in a 0.1 M electrolyte solution of TBAH in anhydrous DMF.

For bulk electrolysis with the alkali salt, solutions were purged with a stream of Ar or $CO_2$ for 15 min after the addition of $KClO_4$. Before the electrolysis, the atmosphere in the cell was replaced with $CO_2$ and electrolysis were conducted with an applied potential of –1.8 V for 1h. The solutions were constantly stirred throughout the experiment.

**Analysis of Gaseous products.** After each control potential electrolysis experiment (CPE), gaseous product generated were investigated by removing a known volume (250 μL) of the headspace gas with a gas tight syringe (Hamilton) injecting them to an Agilent Technologies 7820A GC system equipped with a thermal conductivity detector. CO production was quantitatively detected using a CP-CarboPlot P7 capillary column (27.46 m in length and 25 μm internal diameter). Temperature was held at 150 °C for the detector and 34 °C for the oven. The carrier gas was helium flowing at 9.5 mL/min at constant pressure of 0.4 bars. Injection was performed via a 250 μL gas-tight (Hamilton) syringe previously degassed with Ar or $CO_2$. Conditions allow detection of $H_2$, $O_2$, $N_2$, CO, and $CO_2$, among other gases. Calibration curves for CO were determined separately by injecting known quantities of pure gas.

**Table S4**. Bulk electrolysis data of **1**.

| **Entry** | **1** (μmoles) | Time (min) | Gas | Charge passed (C) | CO formed (μmoles) | $KClO_4$ | Potential (V) |
|---|---|---|---|---|---|---|---|
| 1 | - | 60 | $CO_2$ | 5.612 | 0 | - | –1.8 |
| 2 | 30 | 60 | Ar | 5.657 | 2.7 | - | –1.8 |
| 3 | 30 | 60 | $CO_2$ | 1.861 | 8.2 | - | –1.8 |
| 4 | 30 | 60 | Ar | 4.548 | 2.6 | 45 mM | –1.8 |
| 5 | 30 | 60 | $CO_2$ | 4.857 | 2.7 | 45 mM | –1.8 |

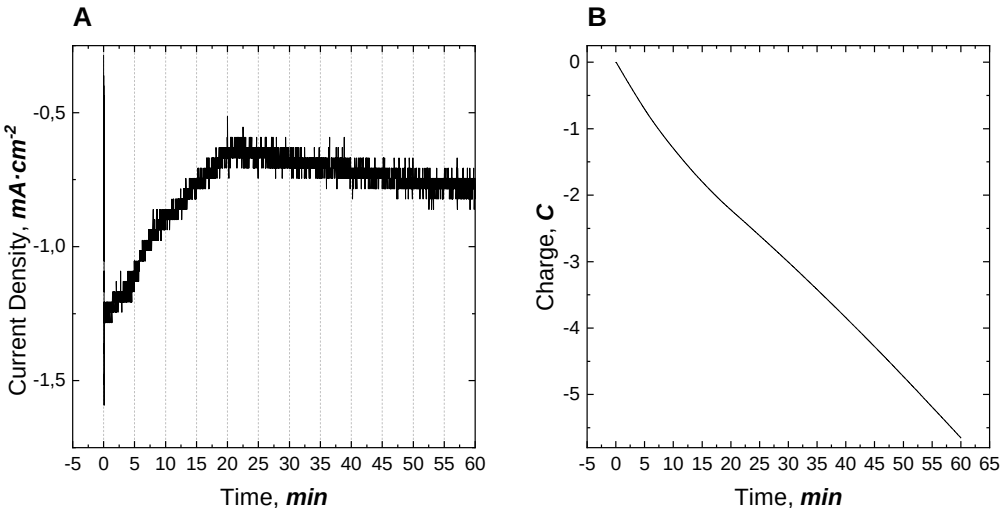


**Figure S38**. Conditions from Entry 2, Table S3: Under Ar atmosphere, 5 mM of **1** in a 0.1 M solution of TBAH in anhydrous DMF (6 mL), at $E_{appl}$ = –1.8 V: **A**, Current passed over 1h of CPE of **1**; **B**, Charge passed over 1 h of CPE of **1**.

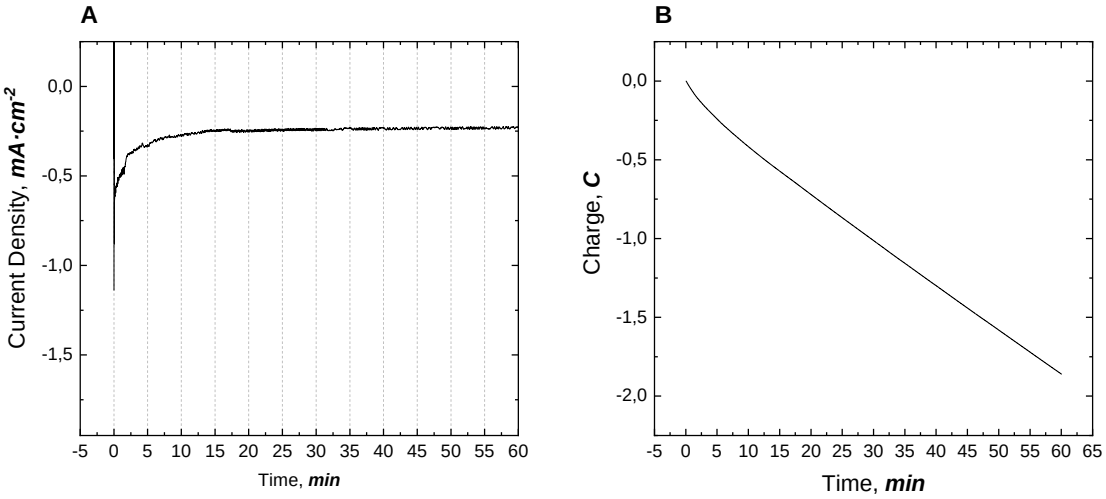


**Figure S39**. Conditions from Entry 3, Table S3: Under $CO_2$ atmosphere, 5 mM of **1** in a 0.1 M solution of TBAH in anhydrous DMF (6 mL), at $E_{appl}$ = –1.8 V: **A**, Current passed over 1 h of CPE of **1**; **B**, Charge passed over 1h of CPE of **1**.

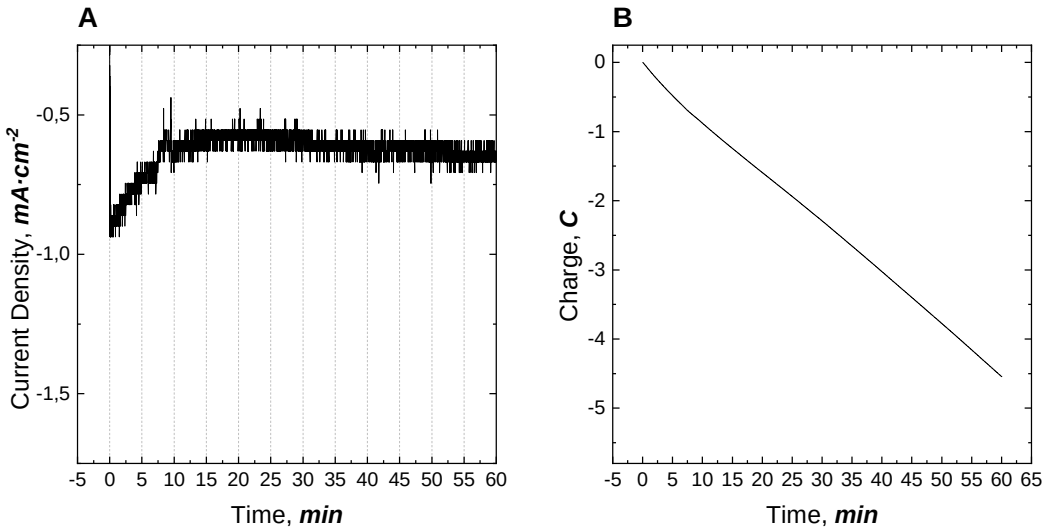


**Figure S40**. Conditions from Entry 4, Table S3: Under Ar atmosphere, 5 mM of **1** in a 0.1 M solution of TBAH in anhydrous DMF (6 mL) containing 45 mM of $KClO_4$, at $E_{appl}$ = –1.8 V: **B**, Current passed over 1 h of CPE of **1**; **B**, Charge passed over 1h of CPE of **1**.

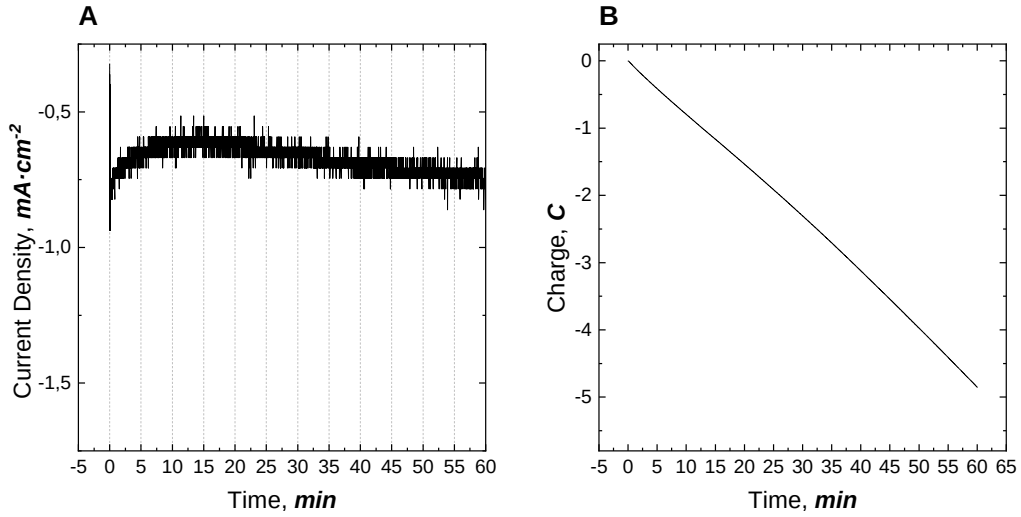


**Figure S41**. Conditions from Entry 5, Table S3: Under $CO_2$ atmosphere, 5 mM of **1** in a 0.1 M solution of TBAH in anhydrous DMF (6 mL) containing 45 mM of $KClO_4$, at $E_{appl}$ = –1.8 V: **A**, , Current passed over 1 h of CPE of **1**; **B**, Charge passed over 1 h of CPE of **1**.

## VI. XPS Analysis

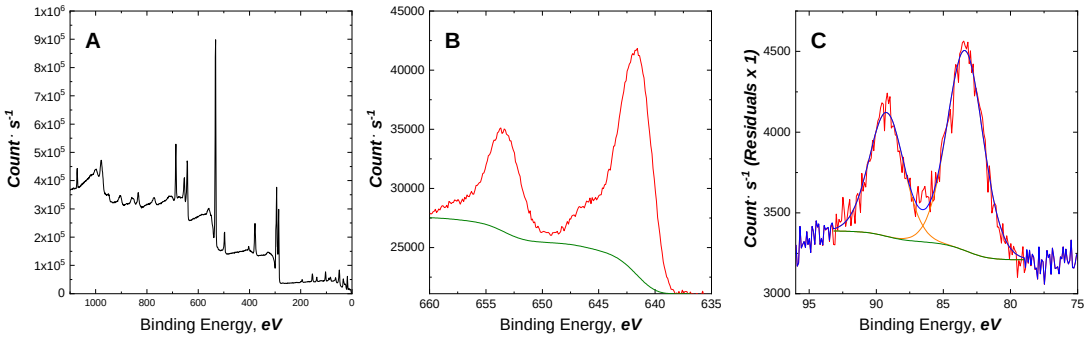


**Figure S42**. **A**, XPS spectra; **B**, Mn2p energy level; **C**, Mn3s energy level at a glassy carbon plate after 1 h CPE experiment. Conditions during deposition: $CO_2$ atmosphere, 5 mM of **1** in a 0.1 M solution of TBAH in anhydrous DMF, at $E_{appl}$ = –1.8 V.

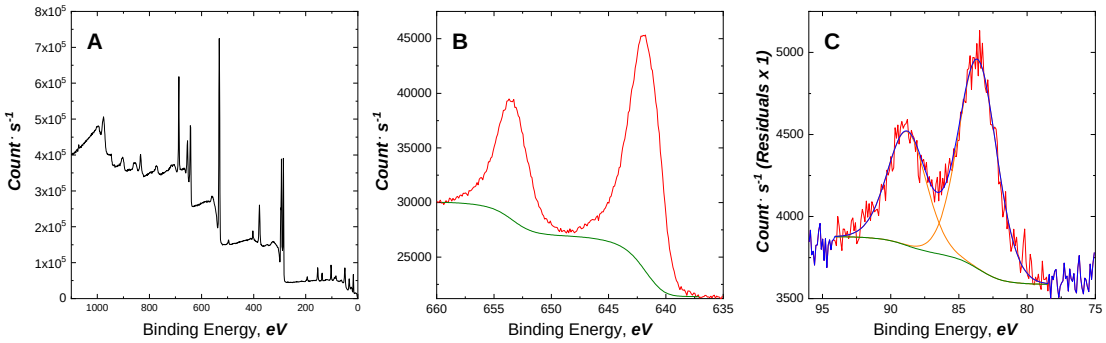


**Figure S43**. **A**, XPS spectra; **B**, Mn2p energy level; **C**, Mn3s energy level at a glassy carbon plate after 1 h CPE experiment. Conditions during deposition: $CO_2$ atmosphere, 5 mM of **1** in a 0.1 M solution of TBAH in anhydrous DMF containing 45 mM of $KClO_4$, at $E_{appl}$ = –1.8 V.

## VII. X-ray Diffraction Analysis

**Crystallography.** Crystallographic data as well data collection and refinement of complex **1** are summarized in Table S4. Selected bond distances and bond angles are given Table S5. Single crystal suitable for X-ray diffraction was selected under immersion oil in ambient conditions and attached to a MiTenGen microloop mounted on thin glass fiber using. Prior to data collection, crystal was cooled to 193(2) K. Data were collected on a Bruker D8 Quest APEX-III single crystal diffractometer using monochromatic radiation λ (Mo Kα1) = 0.71073 Å by a IμS 3.0 microfocus X-ray source. The diffraction images collected were processed and scaled using APEX-III software (Apex3 v2016.9-0, Bruker, 2016). The structures were solved with SHELXT and was refined against $F^2$ on all data by full-matrix least squares with SHELXL.[3] Systematic absences in the diffraction data and unit-cell parameters were consistent with tetragonal $P4_12_12$ (No. 92) for complex **1.** All non-hydrogen atoms were refined anisotropically. Hydrogen atoms were included in the model at geometrically calculated positions and refined using a riding model, unless otherwise noted. The isotropic displacement parameters of all hydrogen atoms were fixed to 1.2 times the U value of the atoms to which they are linked (1.5 times for methyl groups).

Data Centre as supplementary publication number CCDC 2001353 (**1**).

**Table S5**. Crystal data and structural refinement details for complex **1**

| | |
|---|---|
| Chemical formula | $C_{28}H_{32}MnN_3O_6$ |
| Formula weight | 561.50 |
| Crystal system | Tetragonal |
| Space group | $P4_12_12$ |
| Temperature (K) | 193(2) |
| *a*, *c* (Å) | 18.495(5), 17.890(6) |
| $\beta$ (°) | 90 |
| *V* (Å$^3$) | 6120(4) |
| *Z* | 8 |
| $\rho_{calc}$ (g/cm$^3$) | 1.219 |
| Crystal size (mm) | 0.18 × 0.14 × 0.07 |
| *F*(000) | 2352 |
| 2$\theta$ range for data collection (°) | 4.404 to 50.126 |
| Limiting indices | –21≤ h ≤ 21,<br>–21≤ k ≤ 19,<br>–21≤ l ≤ 21, |
| Reflections collected/unique | 43454/ 5395 |
| Absorption correction | Multi-scan |
| $T_{min}$, $T_{max}$ | 0.594, 0.745 |
| Data/restraints/parameters | 5395/0/349 |
| Goodness-of-fit on F$^2$ | 1.042 |
| Final R indexes [I> 2σ (I)] | $R_1$ = 0.0709, w$R_2$ = 0.1593 |
| $R_{int}$ | 0.188 |
| (sin q/l)$_{max}$ (Å$^{-1}$) | 0.596 |
| Largest diff. peak/hole (eÅ$^{-3}$) | 0.75/ –0.33 |
| Flack parameter | 0.03(2) |

**Table S6**. Selected bond distance (Å) and angles (°) for **1** at 193 K

| | |
|---|---|
| Mn1—C23 | 1.823(10) |
| Mn1—C21 | 1.841(11) |
| Mn1—C24 | 1.857(9) |
| Mn1—C22 | 1.860(11) |
| Mn1—C6 | 2.002(8) |
| Mn1—N1 | 2.070(7) |
| O4—C23 | 1.140(11) |
| O1—C1 | 1.272(10) |
| O5—C24 | 1.136(10) |
| O3—C22 | 1.151(12) |
| O2—C21 | 1.157(12) |
| C23—Mn1—C21 | 91.9 (4) |
| C23—Mn1—C24 | 89.1 (4) |
| C21—Mn1—C24 | 90.2 (4) |
| C23—Mn1—C22 | 90.6 (5) |
| C21—Mn1—C22 | 177.4 (4) |
| C24—Mn1—C22 | 90.6 (4) |
| C23—Mn1—C6 | 97.2 (4) |
| C21—Mn1—C6 | 88.4 (4) |
| C24—Mn1—C6 | 173.6 (4) |
| C22—Mn1—C6 | 90.6 (4) |
| C23—Mn1—N1 | 173.9 (3) |
| C21—Mn1—N1 | 89.9 (4) |
| C24—Mn1—N1 | 96.7 (3) |
| C22—Mn1—N1 | 87.5 (4) |
| C6—Mn1—N1 | 77.1 (3) |
| O5—C24—Mn1 | 171.4 (8) |
| O3—C22—Mn1 | 179.5 (9) |
| O2—C21—Mn1 | 179.1 (10) |

1. A. D. Bain, *Progress in Nuclear Magnetic Resonance Spectroscopy*, 2003, **43**, 63-103.
2. L. Fielding, *Tetrahedron*, 2000, **56**, 6151-6170.
3. G. Sheldrick, *Acta Crystallographica Section A*, 2008, **64**, 112-122.